3-2024

New geochemical and geochronological insights on forearc magmatism across the Sanak-Baranof belt, southern Alaska: A tale of two belts

Adrian A. Wackett
Trinity University

Diane R. Smith
Trinity University

Cameron Davidson
Carleton College

John I. Garver
Union College - Schenectady, NY

Repository Citation

Adrian A. Wackett, Diane R. Smith, Cameron Davidson, John I. Garver; New geochemical and geochronological insights on forearc magmatism across the Sanak-Baranof belt, southern Alaska: A tale of two belts. Geosphere 2024; 20 (2): 451–475. doi: https://doi.org/10.1130/GES02642.1

Research Paper

GEOSPHERE

GEOSPHERE, v. 20, no. 2

https://doi.org/10.1130/GES02642.1

13 figures; 2 tables; 1 set of supplemental files

CORRESPONDENCE: dsmith@trinity.edu

CITATION: Wackett, A.A., Smith, D.R., Davidson, C., and Garver, J.I., 2024, New geochemical and geochronological insights on forearc magmatism across the Sanak-Baranof belt, southern Alaska: A tale of two belts: Geosphere, v. 20, no. 2, p. 451–475, https://doi.org/10.1130/GES02642.1.

Science Editor: Christopher J. Spencer
Associate Editor: Eric H. Christiansen

Received 25 January 2023
Revision received 13 August 2023
Accepted 17 January 2024

Published online 8 March 2024

New geochemical and geochronological insights on forearc magmatism across the Sanak-Baranof belt, southern Alaska: A tale of two belts

Adrian A. Wackett[1,2], Diane R. Smith[1], Cameron Davidson[3], and John I. Garver[4]

[1]Department of Geosciences, Trinity University, San Antonio, Texas 78212, USA
[2]Department of Earth and Planetary Sciences, Stanford University, Stanford, California 94305, USA
[3]Department of Geology, Carleton College, Northfield, Minnesota 55057, USA
[4]Geosciences Department, Union College, Schenectady, New York 12308, USA

ABSTRACT

The Sanak-Baranof belt includes a series of near-trench plutons that intrude the outboard Chugach–Prince William terrane over ~2200 km along the southern Alaskan margin. We present new petrological, geochronological, and geochemical data for comagmatic microgranitoid enclaves and granitoid rocks from the Crawfish Inlet (ca. 53–47 Ma) and Krestof Island (ca. 52 Ma) plutons on Baranof and Krestof Islands, as well as the Mount Stamy (ca. 51 Ma) and Mount Draper (ca. 54–53 Ma) plutons and associated mafic rocks that intrude the Boundary block at Nunatak Fiord near Yakutat, Alaska, USA. These data suggest that intrusion of the Sanak-Baranof belt plutons is actually a tale of two distinct belts: a western belt with crystallization ages that young systematically from west to east (63–56 Ma) and an eastern belt with crystallization ages ranging from 55 to 47 Ma, but with no clear age progression along the margin. Hf isotope analyses of magmatic zircon from the western Sanak-Baranof belt become increasingly evolved toward the east with $\varepsilon Hf_t = 9.3 \pm 0.7$ on Sanak Island versus $\varepsilon Hf_t = 5.1 \pm 0.5$ for the Hive Island pluton in Resurrection Bay. The Hf isotope ratios of eastern Sanak-Baranof belt rocks also vary systematically with age but in reverse, with more evolved ratios in the oldest plutons ($\varepsilon Hf_t = +4.7 \pm 0.7$) and more primitive ratios in the youngest plutons ($\varepsilon Hf_t = +13.7 \pm 0.7$). We propose that these findings indicate distinct modes of origin and emplacement histories for the western and eastern segments of the Sanak-Baranof belt, and that the petrogenesis of eastern Sanak-Baranof belt plutons (emplaced subsequent to 57–55 Ma) was associated with an increasing mantle component supplied to the youngest eastern Sanak-Baranof belt magmas. These plutons reveal important information about offshore plate geometries and a dynamic period of plate reorganization ca. 57–55 Ma, but a clearer picture of the tectonic setting that facilitated these Sanak-Baranof belt intrusions cannot be resolved until the magnitude and significance of lateral translation of the Chugach–Prince William terrane are better understood.

INTRODUCTION

The continental framework of southern Alaska has been incrementally constructed and modified over the past ~200 m.y. by a complex history of accretion, strike-slip faulting, metamorphism, and plutonism (Hudson et al., 1979; Plafker et al., 1994; Colpron et al., 2007; Garver and Davidson, 2015). Accretion of the outboard Chugach–Prince William terrane to the Wrangellia composite terrane (Wrangellia, Peninsular, and Alexander terranes) resulted in one of the largest accretionary complexes in the world (Fig. 1), with the majority of its growth occurring during Late Cretaceous and early Paleocene time (Plafker, 1990; Plafker et al., 1994). This intensive accretionary period was concomitant with dextral strike-slip translational displacement of the outboard Chugach–Prince William terrane along the ~2000-km-long Border Ranges fault system (Fig. 1; MacKevett and Plafker, 1974; Pavlis et al., 1988, 2003; Little and Naeser, 1989; Pavlis and Roeske, 2007), further complicating paleo-reconstructions. Resolving the dynamics of this accretionary episode and constraining the paleogeography of the outboard Chugach–Prince William terrane, in particular, remain outstanding questions in Cordilleran tectonics.

There are several competing hypotheses concerning the paleoposition and formation of the Chugach–Prince William terrane along the Cordilleran margin (for review, see Fuston and Wu, 2021). The first, termed the "Resurrection plate hypothesis," posits that the Sanak-Baranof belt intruded the Chugach–Prince William terrane more or less in situ (Haeussler et al., 2003). In this scenario, the series of biotite tonalite, granodiorite, and granite plutons that intrude the Chugach–Prince William terrane over ~2200 km are explained by the eastward migration of the Kula-Resurrection spreading ridge, associated with the long-since-subducted Resurrection plate, and the near-trench plutons in the Pacific Northwest were formed from interaction with the Resurrection-Farallon Ridge (Haeussler et al., 2003). This hypothesis requires that ridge-trench

Diane Smith https://orcid.org/0000-0002-2029-0709

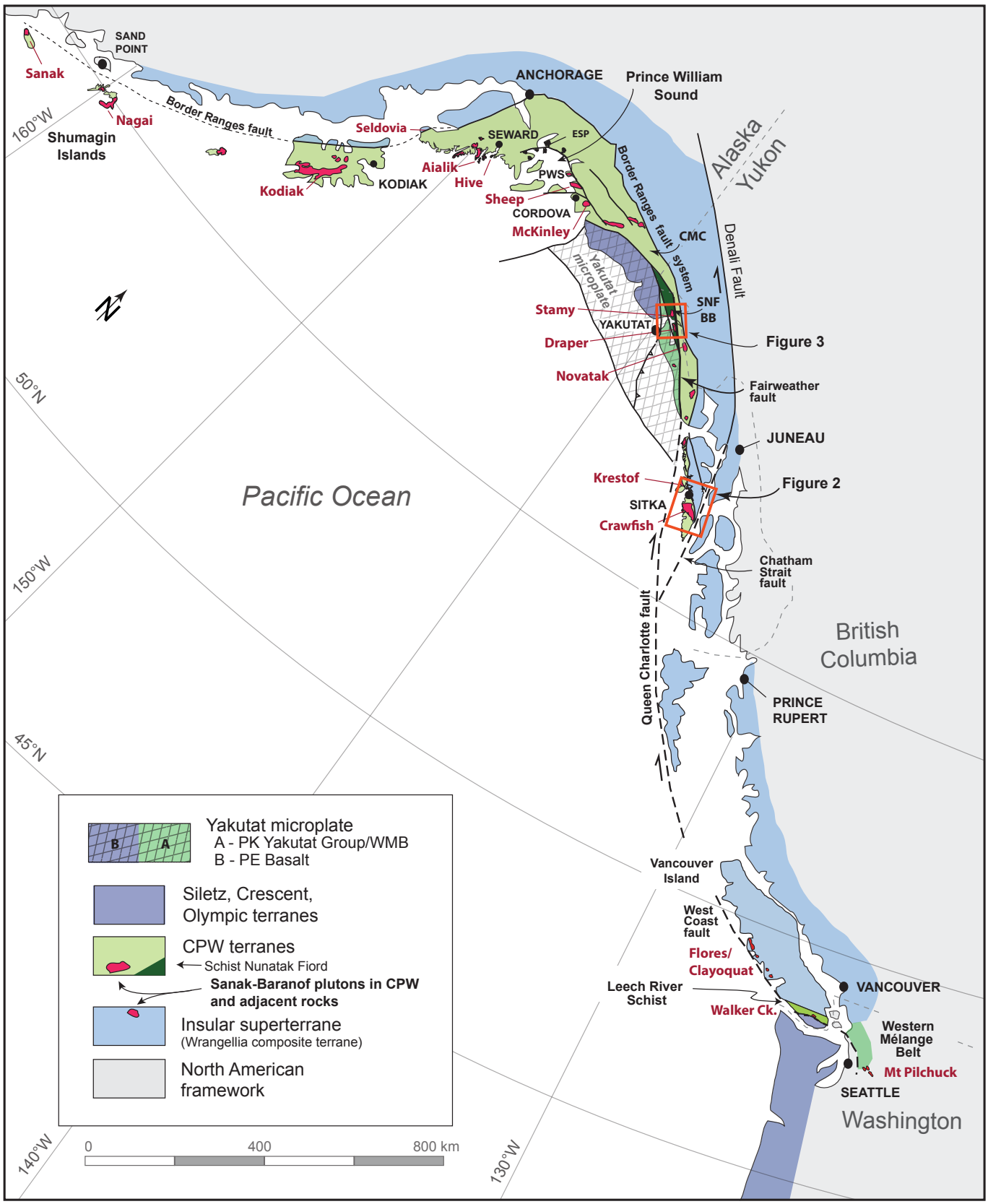

Figure 1. Schematic tectonic map of the modern-day Cordilleran margin stretching from the southwestern Alaskan margin at Sanak Island to northern Washington State (modified after Cowan, 2003). Abbreviations are as follows: PWS—Prince William Sound; ESP—Eshamy Suite plutons; CMC—Chugach metamorphic complex; SNF BB—schist of Nunatak Fiord in the Boundary block; Ck.—Creek; CPW—Chugach–Prince William terrane. Inset boxes identify locations of the maps illustrated in Figures 2 and 3. PK—Paleocene-Cretaceous; PE—Paleocene-Eocene; WMB—Western Mélange Belt (in the Cascades).

interactions occurred simultaneously in two different places, and it requires that paleomagnetic data from host rocks of the Chugach–Prince William terrane be rejected. In the alternative "Baranof–Leech River" hypothesis (Cowan, 1982, 2003), the Chugach–Prince William terrane formed far to the south, making the schist and turbidites of the Chugach–Prince William terrane at Baranof Island contiguous with the Leech River Schist exposed on southern Vancouver Island (Fig. 1). In this scenario, the anomalous near-trench plutons that intrude the Chugach–Prince William terrane were all generated by a single ridge to the south. Following intrusion, some of these plutons experienced northward transport along with the Chugach–Prince William terrane north of the Kula-Farallon Ridge positioned at ~48°N–49°N paleolatitude (Cowan, 1982, 2003). Other ridge-trench subduction models are similar in scope but differ in their proposed Kula-Farallon plate configurations, and in their possible involvement with the Yellowstone hotspot (Engebretson et al., 1985; Bradley et al., 2003; Clennett et al., 2020; Fuston and Wu, 2021; Geen and Canil, 2023).

Two important and influential paleomagnetic data sets emerged early on that bear directly on the paleoposition of the Chugach–Prince William terrane and, by implication, the intruding Sanak-Baranof belt plutons. One shows that pillow basalts of the Paleocene Ghost Rocks Formation (part of Chugach–Prince William terrane) on Kodiak Island experienced 25° ± 7° poleward displacement (Plumley et al., 1983; Moore et al., 1983), and another suggests that pillows and sheeted dikes of the Prince William terrane exposed on the Resurrection Peninsula (Kenai Peninsula) experienced 13° ± 9° poleward displacement (Bol et al., 1992). Thus, the ensuing ridge-trench intersection models that considered the paleomagnetic data suggested that Sanak-Baranof belt plutonism occurred well to the south of Alaska, USA, followed by coastwise translation of the Chugach–Prince William terrane and Sanak-Baranof belt following pluton emplacement (e.g., Bradley et al., 1993; Sisson and Pavlis, 1993; Haeussler et al., 1995; Pavlis and Sisson, 1995).

Regardless of which hypothesis is favored for the Chugach–Prince William terrane, there are several key observations and assumptions embedded within essentially all previous studies considering the Sanak-Baranof belt and its tectonic implications. These include: (1) The Sanak-Baranof belt plutons are time-transgressive and become younger systematically toward the east (e.g., Bradley et al., 2003; Farris and Paterson, 2009); (2) the same tectonic mechanism (crustal anatexis in a thickened accretionary wedge and/or ridge-trench intersection and slab window development) was responsible for generating the Sanak-Baranof belt plutons (Marshak and Karig, 1977; Hudson et al., 1979); and (3) through these lines of reasoning, the Sanak-Baranof belt encompasses a coherent set of petrogenetically related rocks across the entire ~2200 km belt, but this intrusive suite is petrologically and tectonically distinct from other near-trench intrusive rocks farther to the south (e.g., rocks intruding the Leech River Schist on southern Vancouver Island; see Groome et al., 2003; Seyler et al., 2022; Geen and Canil, 2023). These assumptions persist despite the near-complete absence of geochronological and/or geochemical data available for Sanak-Baranof belt intrusive rocks spanning >400 km between the Boundary block at Nunatak Fiord near Yakutat and Baranof Island at the purported easternmost periphery of the belt. Another critical source of uncertainty is the amount of movement by strike-slip displacement within the Chugach–Prince William terrane itself, which would obscure the original distance between Sanak-Baranof belt plutons at the time of intrusion. For example, there are indications that this offset may be particularly pronounced for Sanak-Baranof belt plutons in the Boundary block, which is west of the Fairweather fault (Fig. 1; Schartman et al., 2019).

Here we present new petrological, geochemical, and geochronological data for magmatic enclaves and their host granitoids from the Crawfish Inlet and Krestof Island plutons on Baranof and Krestof Islands near Sitka, Alaska. We present this detailed characterization of Crawfish Inlet and Krestof Island intrusive rocks alongside a comparable data set for the Mount Stamy and Mount Draper plutons and affiliated mafic rocks that intrude the Boundary block at Nunatak Fiord near the town of Yakutat, Alaska. We also report new U-Pb crystallization ages and εHf_t analyses of magmatic zircons from select Sanak-Baranof belt intrusive rocks west of the Boundary block to facilitate comparisons on a belt-wide scale, as well as new εHf_t measurements on detrital zircons collected from the Chugach–Prince William sedimentary rocks that host the near-trench Sanak-Baranof belt plutons across the southern Alaskan margin.

REGIONAL GEOLOGIC SETTING

The Chugach–Prince William terrane and outboard Yakutat microplate make up the extensive and complexly deformed Mesozoic to early Cenozoic accreted terranes that are now situated along the southern margin of Alaska (Fig. 1; Plafker et al., 1989, 1994; Bradley et al., 2003; Colpron et al., 2007; Garver and Davidson, 2015). The Chugach–Prince William composite terrane encompasses both the Chugach and Prince William terranes and is composed largely (~90%) of Campanian–Maastrichtian to Eocene turbidites and oceanic metabasalts (Plafker et al., 1989, 1994; Farmer et al., 1993; Garver and Davidson, 2015; Davidson and Garver, 2017). The primary turbidite facies[1] of the Chugach terrane (predominantly Campanian–Maastrichtian in age) stretch roughly 2200 km from Sanak Island in the west to Baranof Island in the east (Fig. 1; Plafker et al., 1994; Bradley et al., 2003; Gasser et al., 2012). The Paleocene–Eocene Prince William terrane, namely the Orca Group, has historically thought to have been exposed primarily in and around the Prince William Sound, but new U-Pb detrital zircon ages with Paleocene maximum depositional ages for metamorphosed turbidites extend the Prince William terrane farther east to southern Baranof Island (Fig. 1; Rick, 2014; Olson et al., 2017). Sandstone composition and zircon provenance are similar for turbidites of the Chugach and Orca Groups, and they are thus treated as one common unit (see discussion in

[1]In the literature, this mainly includes the Shumagin Formation, Kodiak Formation, Valdez Group, and part of the Sitka Graywacke.

Garver and Davidson, 2015). However, a primary difference between the two is that the Orca Group has significant packages of mafic volcanic rocks that appear to be locally associated with ophiolites (Lytwyn et al., 1997; Davidson and Garver, 2017). East and south of Prince William Sound, amphibolites (±garnet) are also common in the schists and gneisses of the Chugach metamorphic complex, which is the high-grade metamorphic equivalent of the Chugach–Prince William terrane (Sisson et al., 1989; Bruand et al., 2011, 2014).

The thick package of imbricated turbidites (structural thickness >30 km) that dominates the Chugach–Prince William terrane is thought to have formed in an accretionary complex adjacent to an active volcanic arc built on or adjacent to early Mesozoic basement rocks (Plafker et al., 1994; Haeussler et al., 2006; Garver and Davidson, 2015). Petrographical and geochemical evidence suggests the source of detritus for the turbidites was a progressively eroded magmatic arc (i.e., the inboard Coast plutonic complex), and that erosion and deep exhumation resulted in extensive sediment accumulation along the continental margin during the Late Cretaceous and early Paleocene (Hollister, 1979; Dumoulin, 1988; Samson et al., 1991; Farmer et al., 1993; Plafker et al., 1994; Garver and Davidson, 2015). Analysis of sandstones from across the belt and ages of detrital zircon from those sandstones indicate broad homogeneity of the clastic materials (Zuffa et al., 1980; Dumoulin, 1988; Garver and Davidson, 2015). From a geochemical perspective, the turbidites of the Chugach–Prince William terrane are similar to the elemental and isotopic compositions of their Coast plutonic complex granitic source (Samson et al., 1991; Farmer et al., 1993; Sample and Reid, 2003).

INTRUSIVE ROCKS OF THE EASTERN SANAK-BARANOF BELT

This study focused primarily on the Mount Stamy, Mount Draper, Krestof Island, and Crawfish Inlet plutons in the easternmost portion of the Sanak-Baranof belt in SE Alaska. We sampled the Crawfish Inlet pluton in detail (Fig. 2; Tables 1 and 2;

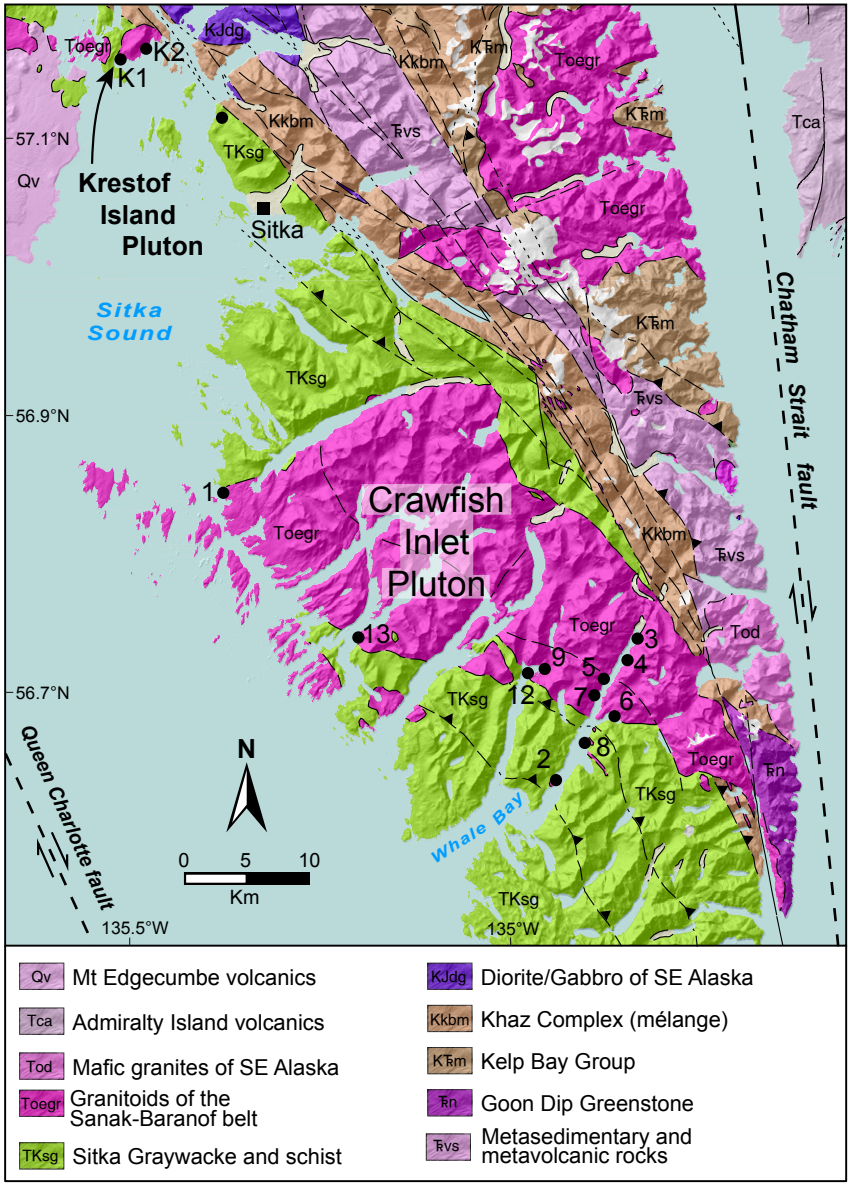

Figure 2. Detailed geologic map of Baranof Island near Sitka, Alaska, USA. Location is depicted by an inset box in Figure 1. Sample locations are shown as small labeled dots with the adjacent numbers corresponding to the sample names listed in Supplemental Table S1 (see text footnote 2). Samples K1 and K2 (KP13–01 and KP13–02) were collected from the Krestof Island pluton located north of Sitka, Alaska. The base map is modified after Wilson et al. (2015).

TABLE 1. Sr AND Nd ISOTOPIC AND GEOCHEMICAL DATA FOR SELECTED BARANOF ISLAND SAMPLES

Sample number	Sample type	Lat	Long	Concentration* (ppm)		Ratio $^{87}Rb/^{86}Sr$	Measured† $^{87}Sr/^{86}Sr$	Initial§ $^{87}Sr/^{86}Sr$	Concentration# (ppm)		Ratio $^{147}Sm/^{144}Nd$	Measured $^{143}Nd/^{144}Nd$	Initial $^{143}Nd/^{144}Nd$	ε_{Nd}**
				Rb	Sr				Sm	Nd				
KP13-01A	Host	57.1572	−135.5250	29	262	0.322	0.705323 ± 6	0.705090	3.48	10.55	0.1426	0.512728 ± 6	0.512680	2.1
KP13-01C	Enclave	57.1572	−135.5250	12	265	0.128	0.705204 ± 5	0.705112	4.65	19.32	0.1456	0.512701 ± 5	0.512652	1.6
KP13-02A	Host	57.1659	−135.4847	48	231	0.602	0.705800 ± 6	0.705365	3.22	14.31	0.1359	0.512645 ± 6	0.512600	0.5
KP13-02B	Enclave	57.1659	−135.4847	32	252	0.363	0.705646 ± 6	0.705384	3.82	14.53	0.1591	0.512655 ± 5	0.512603	0.6
KP13-02C	Enclave	57.1659	−135.4847	39	244	0.465	0.705743 ± 9	0.705408	3.75	14.43	0.1571	0.512658 ± 6	0.512606	0.7
CP13-03A	Host	56.7398	−134.8312	61	434	0.406	0.704832 ± 6	0.704539	3.48	20.36	0.1033	0.512768 ± 4	0.512734	3.1
CP13-03C	Enclave	56.7403	−134.8312	59	326	0.523	0.704592 ± 6	0.704214	2.86	14.41	0.1200	0.512801 ± 5	0.512761	3.7
CP13-03D	Enclave	56.7403	−134.8303	67	392	0.497	0.704555 ± 6	0.704196	2.74	13.38	0.1239	0.512824 ± 6	0.512783	4.1
CP13-07A	Host	56.7013	−134.8856	74	367	0.582	0.705283 ± 6	0.704863	1.81	8.40	0.1302	0.512737 ± 6	0.512694	2.4
CP13-07D	Enclave	56.7013	−134.8856	55	721	0.220	0.703699 ± 6	0.703540	4.94	29.70	0.1005	0.512996 ± 5	0.512962	7.6
CP13-09A	Host	56.7180	−134.9541	66	342	0.560	0.704804 ± 6	0.704400	2.17	9.89	0.1325	0.512816 ± 4	0.512772	3.9
CP13-09C	Enclave	56.7180	−134.9541	49	336	0.425	0.704689 ± 6	0.704382	1.84	8.85	0.1258	0.512810 ± 5	0.512768	3.8
CP13-12A	Host	56.7151	−134.9752	69	329	0.611	0.704734 ± 7	0.704293	1.83	8.33	0.1329	0.512827 ± 8	0.512783	4.1
CP13-12C	Enclave	56.7151	−134.9752	66	346	0.548	0.704507 ± 6	0.704111	0.94	2.86	0.1997	0.512853 ± 5	0.512787	4.2

Notes: Decay constants used were 4.88×10^9 yr and 1.06×10^{11} yr for Rb-Sr and Sm-Nd systematics, respectively.
*Concentrations from X-ray fluorescence (XRF) analyses obtained at Washington State GeoAnalytical laboratory. Values for Rb and Sr are considered accurate to 5% above 1–3 ppm.
†Errors on $^{87}Sr/^{86}Sr$ and $^{143}Nd/^{144}Nd$ measurements are 2σ absolute standard errors that refer to the last significant figures. The mean $^{87}Sr/^{86}Sr$ value for the NBS987 standard over the analytical period was 0.71023 ± 0.00001. The $^{87}Sr/^{86}Sr$ sample ratios were corrected for mass fractionation using the exponential correction factor based on $^{88}Sr/^{86}Sr = 8.375209$ and adjusted for the accepted isotopic composition for NBS987 of $^{87}Sr/^{86}Sr = 0.710248$. Nd and Sm data were corrected for analytical fractionation based on $^{146}Nd/^{144}Nd = 0.7219$, $^{152}Sm/^{147}Sm = 1.783078$, $^{144}Sm/^{147}Sm = 0.206700$, and $^{155}Gd/^{152}Gd = 0.013510$. The mean $^{143}Nd/^{144}Nd$ value for repeated analyses of the Ames Nd standard over the study period was 0.51208 ± 0.00001 (2σ).
§Initial $^{87}Sr/^{86}Sr$ and $^{143}Nd/^{144}Nd$ values were calculated at 50.8 Ma using elemental concentrations determined by XRF and isotope dilution methods, respectively.
#Errors (±2σ) on concentrations determined by isotope dilution methods were less than 0.5% for Nd and 0.4% for Sm.
**ε_{Nd} was calculated at 50.8 Ma assuming the present-day uniform reservoir composition $^{143}Nd/^{144}Nd_{(CHUR)} = 0.512638$ and $^{147}Sm/^{144}Nd_{(CHUR)} = 0.1967$, where CHUR indicated chondritic uniform reservoir.

Table S1[2]), with the goal of evaluating geochemical and geochronological characteristics within a single eastern Sanak-Baranof belt intrusive body. We also conducted investigations and sampling of various plutons from across the remainder of the Sanak-Baranof belt (mainly west of Yakutat), including the Sanak, Nagai, Aialik, Hive Island, Sheep Bay, McKinley Peak, and Novatak Glacier plutons (Fig. 1; Lempert et al., 2015; Arntson et al., 2017).

The Crawfish Inlet pluton intrudes the Cretaceous to Paleocene Sitka Graywacke and its metamorphically equivalent schist of Baranof Island ("Baranof schist;" Rick, 2014), and it is exposed over 560 km² on southern Baranof Island (Fig. 2; Loney et al., 1975). The compositionally similar Redfish Bay pluton on the southern tip of Baranof Island is thought to be connected to the Crawfish Inlet pluton at shallow depths, making this system one of the largest composite batholiths in the Sanak-Baranof belt (Loney et al., 1975; Zumsteg et al., 2003). In addition, there are several small sills and plugs (i.e., "satellites") that occur southwest of the main body of the Crawfish Inlet pluton (e.g., locations 12 and 13 in Fig. 2; Loney et al., 1975). The Krestof Island pluton is located ~40 km northwest of the Crawfish Inlet pluton and is exposed over ~80 km² (Fig. 2). Although the exposed area of the Krestof Island pluton is relatively small, the pluton may be only partially exposed; its unexposed body is believed to be more expansive and may connect to other Eocene plutons on nearby Kruzof Island to the southwest (see fig. 3 in Loney et al., 1975). In comparison to the Crawford Inlet and Krestof Island plutons, smaller exposures of the Mount Stamy and Mount Draper plutons (Hudson et al., 1977) intrude the schist of Nunatak Fiord (informal name; see Richter et al., 2006) in the Boundary block (Fig. 3). Approximately 5 km east of the Mount Draper pluton, there is a small (<10 km²) exposure of mafic intrusions with complex crosscutting relationships, colloquially known as "the Nunatak" (Sisson et al., 2003b). The schist of Nunatak Fiord is composed of Chugach–Prince William rocks that are compositionally similar to turbidites elsewhere in the belt (Schartman et al., 2019), but here they are metamorphosed to greenschist and amphibolite grade (Sisson et al., 2003a, 2003b).

[2]Supplemental Material. All materials along with the raw data and associated R code for reproducing statistical analyses and figures are available for download at https://doi.org/10.1130/GEOS.S.25282339, https://doi.org/10.5281/zenodo.8241978, and from the first author's personal GitHub page (https://github.com/adrianwackett/M006-wackett-SBB-geochem).

FIELD SAMPLING

Sampling sites were restricted to well-exposed and nearly continuous outcrops at sea level, with

TABLE 2. ZIRCON U-Pb GEOCHRONOLOGY AND Hf ISOTOPE DATA FOR SELECTED SANAK-BARANOF BELT SAMPLES

Sample number	Location (WGS 84)			U-Pb age				εHf_t*			
	Pluton	Lat	Long	Age (Ma)	±	MSWD	*n*	εHf_t	±	MSWD	*n*
SI12-02	Sanak Island	54.4868	–162.8146	63.1	0.9	0.248	22/22	9.3	0.7	3.07	15
NIAS12-21A	Nagai Island	55.0397	–160.0815	61.7	0.7	0.750	23/24	8.8	0.7	2.20	15
NI12-05	Nagai Island	55.1160	–160.0250	62.6	0.7	1.285	24/25	N.D.	N.A.	N.A.	N.A.
RB13-04†	Aialik Peninsula	59.8094	–149.6088	56.5	1.0	0.512	28/28	5.9	0.5	3.33	15
RB14-01†	Hive Island	59.8853	–149.3812	56.4	1.5	0.087	26/33	5.1	0.5	7.32	15
CV14-08†	Sheep Bay	60.7105	–146.0894	54.8	0.7	0.393	24/26	4.8	0.5	2.65	15
TI10-02†	Sheep Bay	60.6909	–145.9687	53.9	0.8	0.236	18/21	N.D.	N.A.	N.A.	N.A.
CV14-07†	McKinley Peak	60.4782	–145.3358	54.5	1.7	0.756	20/24	7.4	0.5	7.44	15
RF16-19A	Mount Stamy	59.9027	–139.3162	51.4	0.7	0.388	35/35	6.8	0.5	1.99	14
RF16-05A	Mount Draper	59.8412	–139.0628	52.8	0.6	0.652	35/35	5.1	0.6	3.12	12
RF16-01A	Mount Draper	59.8411	–139.1523	53.1	0.7	0.821	24/28	N.D.	N.A.	N.A.	N.A.
RF16-30A	Mount Draper	59.8413	–139.1838	54.0	0.6	0.241	34/34	7.6	0.3	7.10	15
RF16-32A	Mount Draper	59.8422	–139.1750	53.9	0.8	0.505	15/28	7.6	0.3	19.85	15
HL19-20	Novatak Glacier	59.5469	–138.4051	52.0	0.5	0.793	97/100	N.D.	N.A.	N.A.	N.A.
KP13-01A	Krestof Island	57.1572	–135.5250	52.1	1.0	0.110	28/28	10.5	0.5	1.64	15
CP13-13	Crawfish Inlet	56.7425	–135.1982	53.1	0.8	0.470	30/30	4.7	0.7	1.81	15
CP13-08D	Crawfish Inlet	56.6656	–134.8975	52.7	0.8	1.640	15/20	N.D.	N.A.	N.A.	N.A.
CP13-01	Crawfish Inlet	56.8469	–135.3807	52.2	0.9	0.240	28/28	N.D.	N.A.	N.A.	N.A.
CP13-07A	Crawfish Inlet	56.7013	–134.8856	51.2	0.9	0.430	26/26	8.2	1.0	1.29	5
CP13-05A	Crawfish Inlet	56.7124	–134.8754	50.5	0.9	0.380	27/28	9.3	0.6	0.78	15
CP13-03A	Crawfish Inlet	56.7403	–134.8303	48.6	1.2	0.220	26/26	12.7	0.6	2.86	15
CP13-04	Crawfish Inlet	56.7239	–134.8461	48.0	1.0	0.150	21/21	12.9	0.6	5.51	15
CP13-09A	Crawfish Inlet	56.7180	–134.9541	47.3	1.2	0.060	23/23	13.7	0.7	1.56	15

Notes: WGS 84—World Geodetic System 1984; MSWD—mean square of weighted deviates; *n*—number of analyses used in weighted mean/total number of analyses; N.D.—not determined; N.A.—not applicable.

*εHf_t values were calculated using sample U-Pb age and present-day uniform reservoir composition of $^{176}Hf/^{177}Hf = 0.282785$ and $^{176}Lu/^{177}Hf = 0.0336$ (from Bouvier et al., 2008).

†Previously published in Davidson and Garver (2017); the date given here for sample TI10-02 is revised and supersedes the previously published date.

one exception. Due to difficulty accessing the pluton interior, large float blocks that are believed to have been derived from the nearby Mount Stamy pluton were collected from a steep drainage that incises directly from the pluton. Figures 2 and 3 show sample locations, and Tables 1 and 2 provide geographic coordinates for each sample (see Supplemental Table S1 for a complete listing). Samples collected from the Crawfish Inlet pluton were designed to capture a transect from the pluton periphery to its interior, which penetrates furthest into the pluton center along the south arm of Whale Bay (Fig. 2).

Field relationships offer evidence of commingling between granitoids and more mafic magmas in many of the eastern Sanak-Baranof belt intrusive suites. Magmatic enclaves are present within the Crawfish Inlet, Krestof Island, and Mount Draper plutons. These magmatic enclaves generally occur in swarms of relatively smaller, roundish masses that possess aphanitic to fine-grained textures relative to their host granitoids (Figs. 4A–4D). A mafic dike that was sampled from within the Mount Draper pluton exhibited a cuspate-lobate contact, suggesting a comagmatic relationship between the dike and host granitoid (Figs. 4E–4F).

PETROGRAPHY

Granitoids of the Krestof Island, Crawfish Inlet, Mount Stamy, and Mount Draper plutons are all medium- to coarse-grained assemblages of plagioclase, K-feldspar, quartz, and lesser biotite. Minor phases in some samples include muscovite, hornblende, garnet, and rare clinopyroxene (Wackett, 2014; Arntson, 2018). Accessory minerals include apatite, zircon, titanite, and opaque oxides.

Enclaves within the Krestof Island, Crawfish Inlet, and Mount Draper plutons are finer grained, appear enriched in ferromagnesian minerals relative to host granitoids (e.g., Figs. 5C–5D vs. Figs. 5A–5B), and exhibit crenulate to diffuse contacts with their hosts (Figs. 5G–5H). The occurrence of acicular apatite (Fig. 5E) in some enclaves indicates rapid magmatic quenching (e.g., Wyllie et al., 1962; Didier, 1973; Vernon, 1984; Webster and Piccoli, 2015). Acicular hornblende occurs in enclaves (Fig. 5C), whereas accessory hornblende in the host granitoid exhibits equant and coarser grains (Fig. 5A). Zoned plagioclase and poikilitic textures

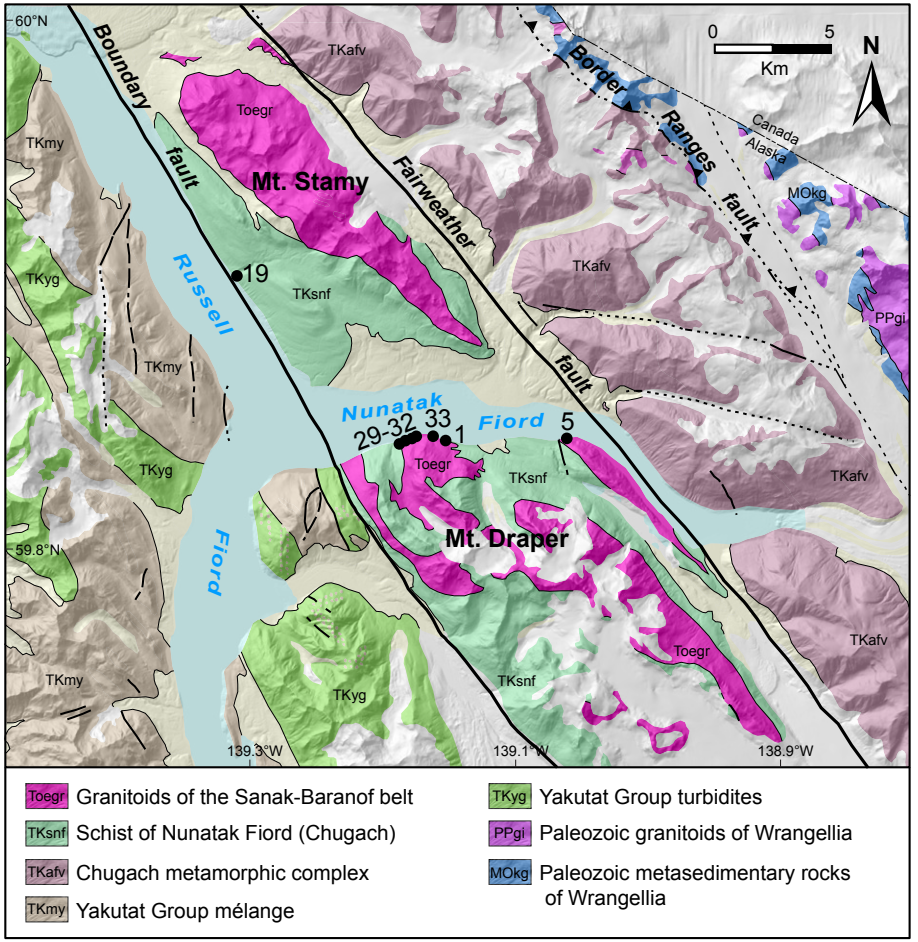

Figure 3. Detailed geologic map of the Nunatak Fiord region near the town of Yakutat, Alaska, USA. The map location is shown by an inset box in Figure 1. The Boundary block is a fault-bounded block comprising the schist of Nunatak Fiord and the Mount Stamy and Mount Draper plutons. The Nunatak is a mafic and highly heterogeneous portion of the Mount Draper pluton (location #5). Sample locations are shown as labeled dots with the numbers corresponding to samples listed in Supplemental Table S1. Sample 19 (RF16–19) was collected from a large debris flow in a drainage that incises the Mount Stamy pluton. Areas in gray (unlabeled geologic units) are ice-covered. The base map is modified from Wilson et al. (2015).

(Fig. 5F) further support a magmatic origin for the enclaves (Vernon, 1984).

Gabbros from "the Nunatak," the large mafic intrusive body adjacent to the Mount Draper pluton (Fig. 3), exhibit subophitic textures with hornblende replacing clinopyroxene in grains surrounding plagioclase. The comagmatic mafic dike emplaced within the Mount Draper pluton contains fine-grained hornblende, plagioclase, and biotite.

ANALYTICAL METHODS

In total, 60 samples from across the Sanak-Baranof belt were selected for major- and trace-element analysis by X-ray fluorescence and inductively coupled plasma–mass spectrometry (ICP-MS) methods at the Washington State University GeoAnalytical Laboratory in Pullman, Washington (Table S1). Details of sample preparation, analytical procedures, and precision/accuracy estimates are available at https://environment.wsu.edu/facilities/geoanalytical-lab/technical-notes/.

Fourteen samples (eight enclaves, six host granitoids; Table 1) from the Crawfish Inlet and Krestof Island plutons were selected for analysis by thermal ionization mass spectrometry for Sr and Nd isotopic compositions at the Jackson School of Geosciences Isotope Geochemistry laboratory, University of Texas–Austin. Details of the analytical procedures used at this laboratory can be found at: www.geo.utexas.edu/isochem/tech_notes/pdf/Sr-Nd-Pb-techniques.pdf. Details of decay constants, analytical errors, age and fractionation corrections, and general isotopic parameters are reported in Table 1.

This study also presents new U-Pb zircon crystallization ages of 23 samples collected from 11 different plutons spanning the entire length of the Sanak-Baranof belt (Table 2). U-Pb and Hf isotope data were collected by laser ablation-ICP-MS (LA-ICP-MS) at the Arizona LaserChron Center following the methods of Gehrels et al. (2008) and Gehrels and Pecha (2014). Details of the analytical methods are provided in Supplemental Tables S2 and S3 for U-Pb and Hf isotopes, respectively. All Hf isotope compositions referenced in the text were corrected for age (εHf_t).

The results for five Sanak-Baranof belt pluton samples reported here were previously published in Davidson and Garver (2017). The complete geochronological data set for Sanak-Baranof belt plutons is available in Table S2. Weighted mean U-Pb dates and concordia diagrams are presented in Figure S1. Backscattered-electron (BSE) and cathodoluminescence (CL) images (Fig. S2) were used to screen for inclusions and inherited cores. Inherited grains were not included when calculating the weighted

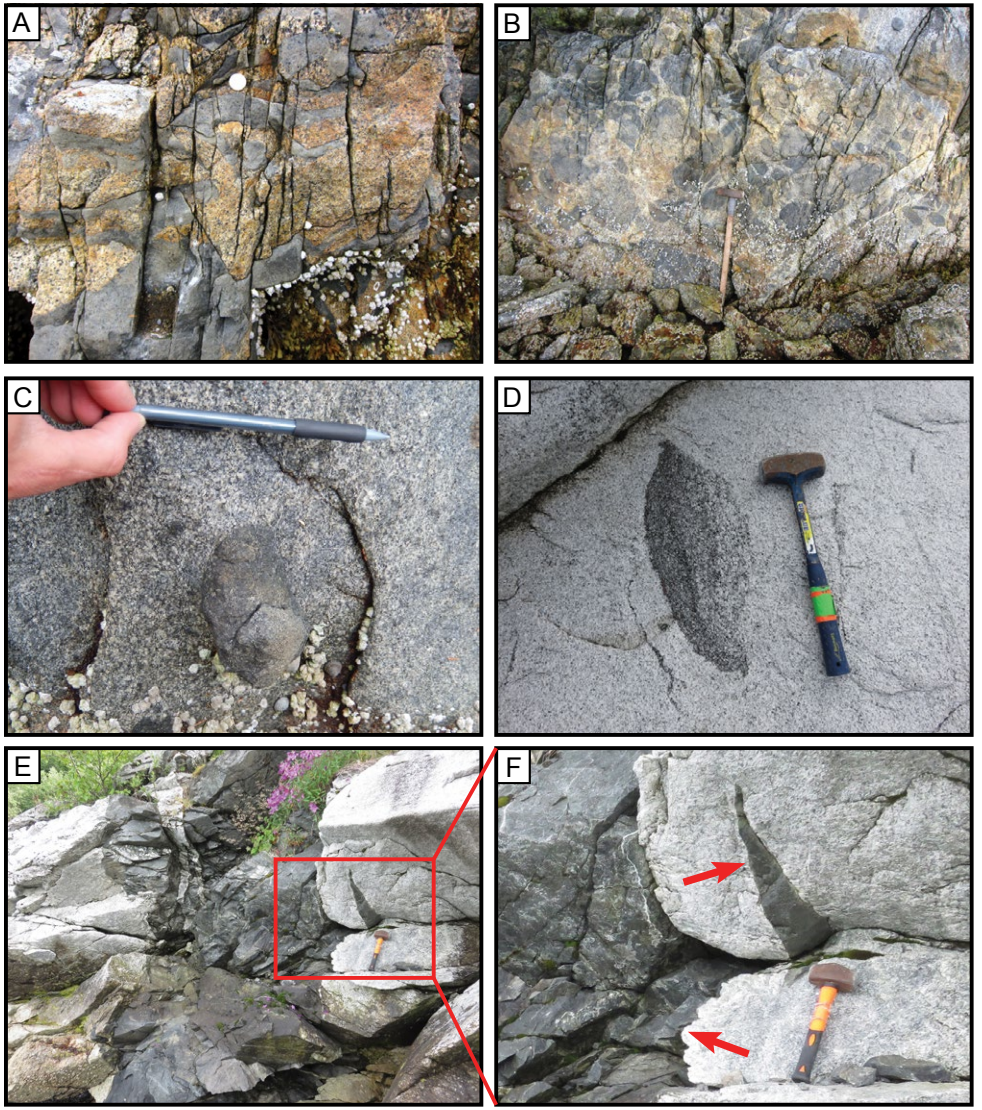

Figure 4. Field photos of select plutons from the eastern Sanak-Baranof belt (Boundary block and Baranof Island area). (A) Mafic enclave swarm in the Crawfish Inlet pluton. Note the cuspate-lobate boundaries between the mafic and felsic rocks; quarter (~2.4 cm diameter) for scale. (B) Mafic enclave swarm emplaced in the Krestof pluton; note the rock hammer (~0.4 m in length) for scale. (C) Typical Krestof Island magmatic enclave exhibiting roundish shape, higher color index, and aphanitic texture relative to its host. (D) Mafic enclave in the Mount Draper host granite. (E) Mutually crosscutting relationships between a mafic dike (sample RF 16–30B) and the Mount Draper pluton. (F) Zoomed image of the panel E inset. Upper red arrow shows an isolated xenolith of the mafic dike in the host granite, and the lower arrow highlights cuspate-lobate texture between the dike and host granite, which indicates a comagmatic relationship.

mean ages reported in Table 2. Weighted mean Hf isotope compositions of zircon from 17 of these samples are also shown in Table 2, with the complete Hf isotope data set provided in Table S3.

We also report detrital zircon Hf isotope data for detrital zircons collected from across the Chugach–Prince William terrane (Table S3 workbook) at localities from the Shumagin Islands (four samples), Seward area (four samples), Prince William Sound (six samples), Boundary block in the Yakutat area (two samples), and Baranof Island (three samples) (see Fig. 1). Because we were interested in the $^{176}Hf/^{177}Hf$ ratio of the sedimentary rocks at the time of intrusion of the Sanak-Baranof belt plutons, the measured $^{176}Hf/^{177}Hf$ ratios in zircon for a given region were recalculated to obtain the ratio at 50 Ma (εHf_{50Ma}), which is the approximate time for the intrusion of the Sanak-Baranof belt plutons. We note that a change of ±10 Ma has a negligible effect on εHf_{50Ma}. For each region (i.e., Shumagin, Seward, Prince William Sound, etc.), 84–184 Hf analyses were taken from the main peaks of the zircon U-Pb age probability distribution of the sedimentary rocks for that region. Because the number of U-Pb analyses is considerably greater than the number of Hf analyses, we created "synthetic" Hf data for the entire U-Pb data set for the region by using the constrained random number generator in Microsoft Excel. This was accomplished by binning the U-Pb dates based on the U-Pb probability distribution plots and then having Excel assign a random Hf ratio between the measured minimum and maximum Hf values for the range of dates in that bin. For Precambrian zircons, we used an empirical linear relationship between U-Pb age and εHf_{50Ma}. An example spreadsheet demonstrating our calculations for the Shumagin Islands region is included in the Table S3 workbook.

The synthetic Hf isotope data were necessary because most samples from the Chugach–Prince William terrane had a dominant Late Cretaceous to Paleocene U-Pb population (or "peak") on the probability distribution plot, with subordinate Jurassic, Paleozoic, and Precambrian populations (see Garver and Davidson, 2015; Davidson and Garver, 2017). However, we typically collected 10 Hf analyses from each of the prominent peaks, regardless

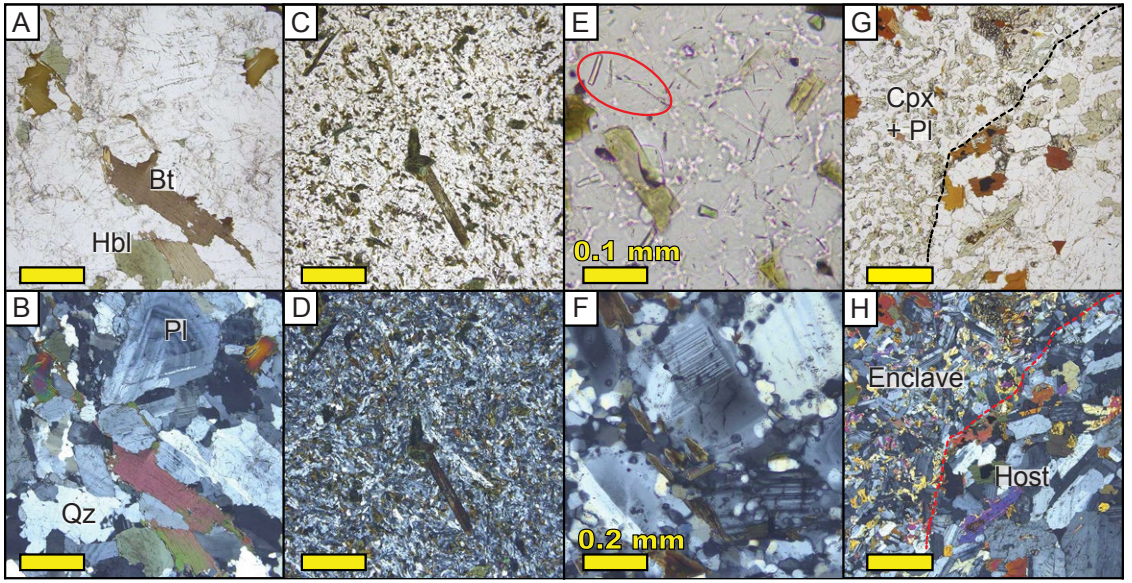

Figure 5. Photomicrographs of selected samples from this study. Unlabeled yellow scale bars are equal to 1 mm, unless otherwise noted. Mineral abbreviations are: Hbl—hornblende; Bt—biotite; Qz—quartz; Pl—plagioclase, Cpx—clinopyroxene. (A) Crawfish Inlet host granitoid (CP13–07A) under plane-polarized light (PPL) and (B) cross-polarized light (XPL). (C) Associated magmatic enclave (CP13–07D) under PPL and (D) XPL. (E) Enclave CP13–07D under high magnification to highlight the presence of acicular apatite crystals (circled in red). (F) Crawfish tonalitic enclave (sample CP13–06B) with a poikilitic texture. (G) Contact between Krestof Island host granitoid (sample KP13–02A) and enclave (sample KP13–02B) shown under PPL and (H) XPL. The enclave is dominated by finer-grained plagioclase and clinopyroxene.

of the number of zircons that made up the peak. Therefore, the synthetic εHf_{50Ma} values were used to obtain a better estimate of the volume of zircon with a given εHf_{50Ma} signature that could potentially be assimilated from Chugach–Prince William sedimentary rocks.

Any additional statistical modeling was conducted using R version 4.2.2 in the R statistical computing environment (R Core Team, 2022). All figures were initially constructed in either R or the IgPet geochemical software (Carr and Gazel, 2017), and final aesthetic modifications were completed in Adobe Illustrator. Thorough details on the statistical methods and full model results are available in Item S1.

WHOLE-ROCK MAJOR- AND TRACE-ELEMENT GEOCHEMISTRY

The Sanak-Baranof belt intrusive rocks include gabbro, gabbroic diorite, diorite, granodiorite, and granite (Fig. 6). For rocks with >60 wt% SiO_2, Barker's (1979) normative anorthite-albite-orthoclase classification scheme suggests that most Sanak-Baranof belt rocks are tonalites, granodiorites, or granites. Two samples from the Crawfish Inlet satellitic bodies are leucogranites due to their low color indices. To simplify discussions, we hereafter refer to all medium- and coarse-grained rocks that host magmatic enclaves and mafic dikes as "granitoids," regardless of whether they classify as tonalites or granodiorites.

Among the plutons studied here, the Mount Draper pluton (n = 11 samples) exhibited the largest range in silica content, with values ranging between ~49 wt% and 74 wt% SiO_2. Samples from the Crawfish Inlet pluton (n = 22) exhibited SiO_2 contents ranging from 56.5 to 75.3 wt%. Excluding the high-silica Crawfish satellite leucogranites (~75 wt% SiO_2), eastern Sanak-Baranof belt granitoids generally exhibited higher CaO, higher Na_2O, and lower K_2O relative to granitoids from the western Sanak-Baranof belt. Mafic samples from the Mount Draper pluton were metaluminous and broadly similar in elemental composition to Alaskan metabasalts and ophiolites of the Prince William terrane (i.e., Orca Group; Fig. 6). Magmatic enclaves from the Krestof Island pluton (open squares) were distinct from their host granitoids (pink filled squares), with SiO_2 contents ranging between ~54 wt% and 56 wt%, compared to ~62–63 wt% for their hosts (Fig. 6). Crawfish Inlet enclaves exhibited a much wider range in SiO_2 contents (~56 wt% to ~72 wt%) that overlaps with the host granitoids, which were between ~66 wt% and 70 wt% SiO_2. The least evolved enclaves from the Krestof Island (open squares) and Crawfish Inlet (open red triangles) (<63 wt% SiO_2) plutons exhibited distinct TiO_2 and P_2O_5 signatures (Fig. 6).

Geochemical distinctions between eastern and western Sanak-Baranof belt granitoids are more clearly defined using trace elements (Figs. 7–9; Table S1). Eastern Sanak-Baranof belt granitoids were generally lower in Sc, La, Th, Zr, and especially Y (as well as Yb, which is not shown here) and were enriched in Sr relative to granitoids from the western Sanak-Baranof belt (Fig. 7). With respect to Th, Sr, La, and Zr, the least evolved (<63 wt% SiO_2) Crawfish Inlet enclaves (red open triangles) again plotted as outliers (Fig. 7). Sr/Y and Ba/Nb ratios generally increased in eastern Sanak-Baranof belt rocks with increasing silica, whereas ratios in western Sanak-Baranof belt rocks remained flat or decreased (Fig. 7).

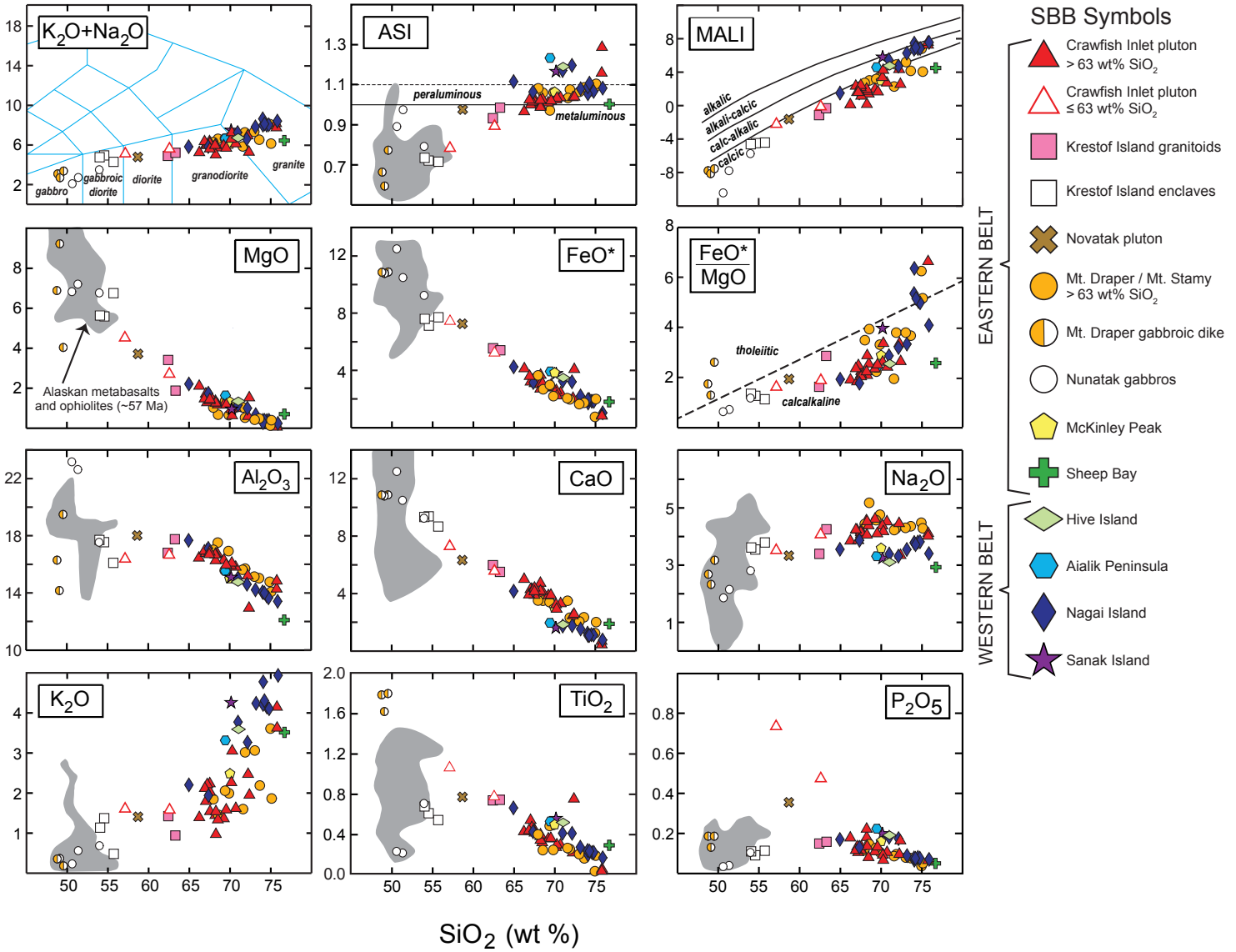

Figure 6. Major- and minor-element Harker diagrams for Sanak-Baranof belt (SBB) intrusive rocks from this study and one sample (S69a) from Hill et al. (1981). The latter sample is geographically proximal to our Sanak Island sample (SI12–02, see Table S1 for details [text footnote 2]), which was collected for zircon analyses but lacks whole-rock elemental geochemistry. Gray fields outline the compositional range of Paleocene–Eocene Alaskan metabasalts and ophiolites (Lull and Plafker, 1990; Lytwyn et al., 1997; Sisson et al., 2003b) for comparison with Sanak-Baranof belt intrusive suites. The total alkalis versus silica classification is from Middlemost (1994). Aluminum saturation index (ASI) is the molecular ratio of $Al_2O_3/[CaO + Na_2O + K_2O]$ (Shand, 1951). The peraluminous-metaluminous boundary (solid line) at ASI = 1.0 is after Shand (1951), and the I-type/S-type boundary (dashed line) at ASI = 1.1 (with S-type >1.1) is after White et al. (1986). MALI is the modified alkali-lime index ($Na_2O + K_2O - CaO$; Frost and Frost, 2008). The boundary between calc-alkaline and tholeiitic suites on the FeO*/MgO diagram is after Miyashiro (1974). Major oxides are given in wt%.

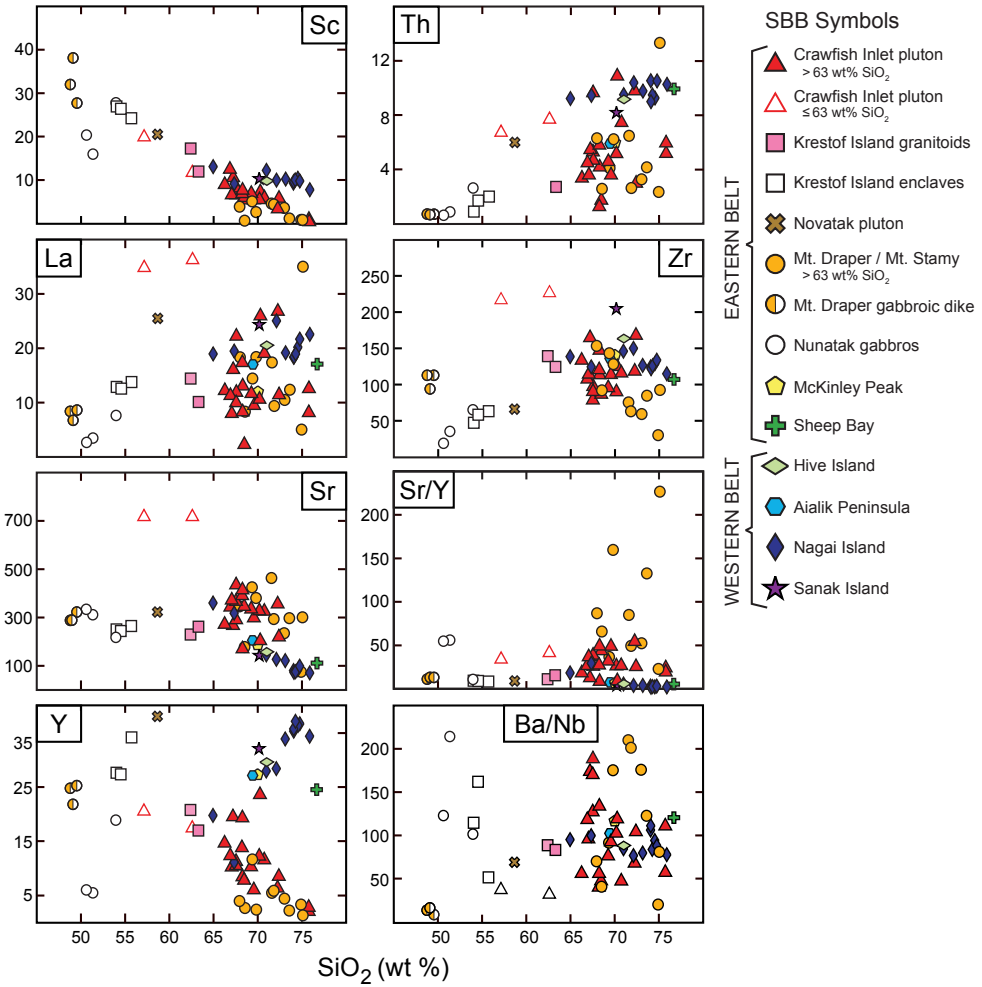

Figure 7. Trace-element (in ppm) Harker diagrams for all new Sanak-Baranof belt (SBB) intrusive rock samples reported in this study.

Normal mid-ocean-ridge basalt (N-MORB)–normalized trace-element patterns (Fig. 8) illustrate that both western and eastern Sanak-Baranof belt granitoids exhibited Nb depletions and Pb enrichments. Ratios of Sr/Y in most western Sanak-Baranof belt rocks and Cordova granitoids were relatively low and overlapped with typical values for N-MORB (Fig. 9). However, a suite of near-trench dikes that intrude the accretionary prism near Seldovia, Alaska (Fig. 9A; Supplemental Material Item S1 and Fig. S1; Lytwyn et al., 2000; Bradley et al., 2003), gave highly variable Sr/Y ratios, with some approaching 175 (plotting off scale in Fig. 9A). The Cordova area plutons (i.e., Sheep Bay, McKinley Peak, Rude River) typically define a small range in Sr/Y from ~4 to 10, with the exception of a late-stage dike that crosscuts the McKinley Peak pluton, which had Sr/Y = 85 (Fig. 9B; Barker et al., 1992). Granitoids from the western Chugach metamorphic complex exhibited a considerable range in Sr/Y values that overlap with adakites (Fig. 9B), with the highest ratio again exhibited by a late-stage dike. The largest range in Sr/Y ratios was observed for the Mount Draper and Mount Stamy plutons in the Boundary block (Fig. 9B; Sisson et al., 2003b), which gave Sr/Y values up to ~200–225 (plotting off scale in Fig. 9B). Crawfish Inlet samples exhibited a moderate range in Sr/Y from ~9 to 55, with many classifying as adakites (Fig. 9C), whereas Krestof Island samples did not classify as adakites. Four eastern Sanak-Baranof belt rocks that plotted at low Sr/Y (<22) and anomalously low Y values (<4 ppm) were particularly high in silica (≥74 wt%). This group included two Mount Draper leucogranite samples (Fig. 9B) and two Crawfish Inlet micaceous garnet-bearing leucogranites (red diamonds; Fig. 9C).

STRONTIUM AND NEODYMIUM ISOTOPE GEOCHEMISTRY

Most eastern Sanak-Baranof belt granitoid rocks and their comagmatic enclaves or affiliated mafic rocks gave εNd_t and $^{87}Sr/^{86}Sr_{initial}$ compositions (Table 1) that closely track end-member mixing curves between N-MORB and average Chugach–Prince William sediments (Figs. 10B–10D). Exceptions are two mafic Nunatak samples (one amphibolite and a gabbro) that were contaminated by crust and/or seawater (Fig. 10C; Sisson et al., 2003b). The coherence of eastern Sanak-Baranof belt rocks to the MORB-sediment mixing curve differs substantially from Sr-Nd isotopic data for the more westerly Kodiak batholith, which largely depart from this mixing curve (Fig. 10A). A Crawfish Inlet enclave with <63 wt% SiO_2 is an outlier among the Baranof Island suite but is isotopically similar to a late-stage felsic dike from Cordova (Fig. 10B) and unaltered rocks from Nunatak Fiord (Fig. 10C). Krestof Island enclaves and granitoids are more isotopically evolved than all Crawfish Inlet samples (Fig. 10D), despite having lower silica contents

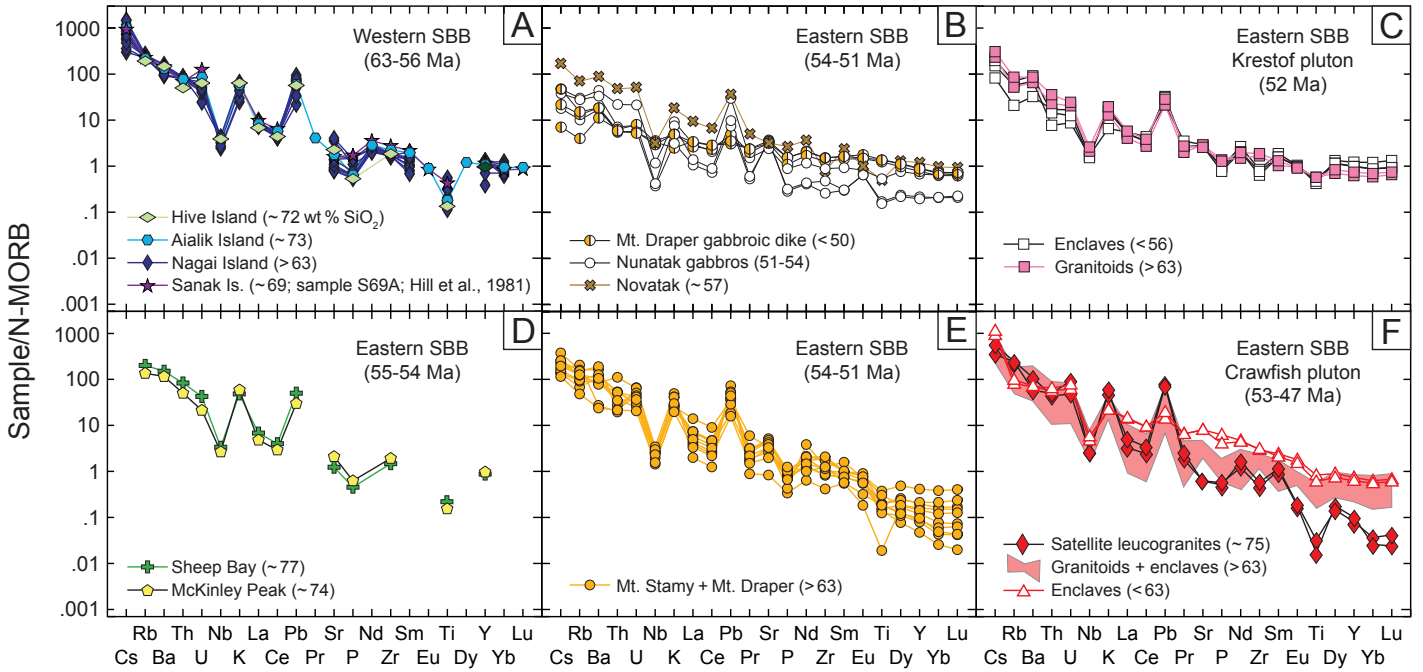

Figure 8. Normal mid-ocean-ridge basalt (N-MORB)–normalized (after Sun and McDonough, 1989) spider diagrams for new Sanak-Baranof belt (SBB) samples reported from this study. Symbols are as in Figures 6, with two exceptions. In panel F, red diamonds are used to distinguish the Crawfish micaceous leucogranite satellites, and the red shaded field represents all Crawfish Inlet samples with >63 wt% SiO_2 (both enclaves and host granitoids). Numbers in parentheses adjacent to the sample labels denote SiO_2 (wt%) values. (A) Spider diagrams for ca. 63–56 Ma western Sanak-Baranof belt rocks stretching from Sanak Island to the Hive Island pluton in Resurrection Bay. (B) One sample from the Novatak Glacier pluton in the Fairweather block plotted alongside mafic compositions from the mafic dike and gabbro that intrude the Boundary block at Nunatak Fiord. (C) Krestof Island pluton (52 Ma) samples. (D) Granitoids from the 55–54 Ma Sheep Bay and McKinley Peak plutons near Cordova, Alaska, USA. Lines are missing where elemental analyses are not available (see Table S1 for details [text footnote 2]). (E) Evolved enclaves and host granitoids (54–51 Ma; >63 wt% SiO_2) from the Mount Stamy and Mount Draper plutons in the Boundary block. (F) Crawfish Inlet pluton samples (53–47 Ma).

(Fig. 6). The Cordova and western Chugach plutonic complexes include late-stage dikes (stars, Fig. 10B) that are isotopically more primitive than rocks from the main plutonic bodies (fields, Fig. 10B).

U-Pb ZIRCON GEOCHRONOLOGY AND Hf ISOTOPE GEOCHEMISTRY

Pluton Crystallization Ages and Hf Isotope Compositions

One sample from the Sanak pluton at the westernmost edge of the Sanak-Baranof belt (Fig. 1) yielded a crystallization age of 63.1 ± 0.9 Ma and a weighted mean εHf_t composition of +9.3 ± 0.7 (Table 2; Fig. 11). Two samples from the Nagai Island pluton (in the Shumagin Islands) recorded statistically indistinguishable ages of 62.6 ± 0.7 Ma and 61.7 ± 0.7 Ma, respectively, and a weighted εHf_t composition of +8.8 ± 0.7. The Aialik and Hive Island plutons near Seward gave nearly identical ages of 56.5 ± 1.0 Ma and 56.4 ± 1.5 Ma, respectively, and εHf_t compositions of +5.9 ± 0.5 and +5.1 ± 0.5 (Fig. 11). The Hive Island pluton contained xenocrysts of kyanite (Kusky et al., 2003; Davidson and Garver, 2017) and yielded seven inherited grains that ranged in age from 361 to 60 Ma (Fig. S1; Table S2). Two samples from the Sheep Bay pluton in eastern Prince William Sound northwest of Cordova, Alaska, yielded overlapping ages of 54.8 ± 0.7 Ma and 53.9 ± 0.8 Ma, and identical εHf_t of +4.8 ± 0.5. One sample from the McKinley Peak pluton east of Cordova recorded an age of 54.5 ± 1.7 Ma and an εHf_t composition of +7.4 ± 0.5 (Table 2; Fig. 11).

More extensive U-Pb age and εHf_t compositional data are available for several plutonic bodies between Yakutat and Baranof Island in the far eastern Sanak-Baranof belt. Four samples from the Mount Draper pluton at Nunatak Fiord yielded closely clustered ages of 54.0 ± 0.6 Ma, 53.9 ± 0.8 Ma, 53.1 ± 0.7 Ma, and 52.8 ± 0.6 Ma with

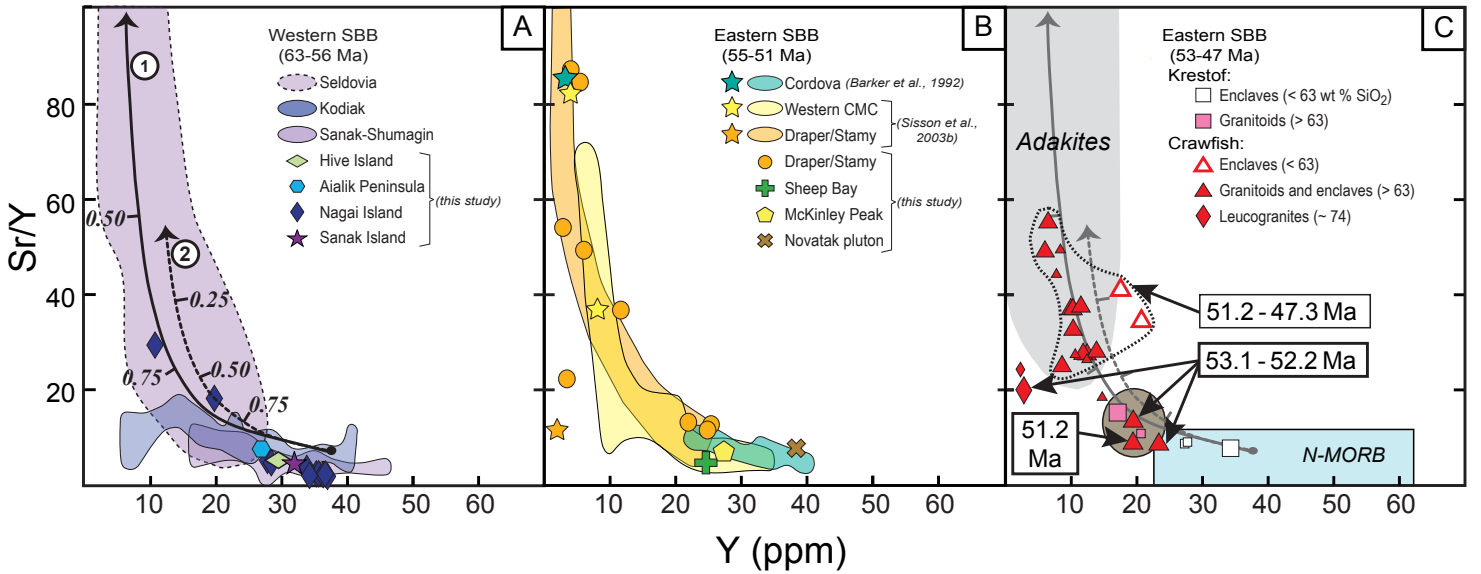

Figure 9. Sr/Y vs. Y (ppm) diagrams for intrusive rocks with >54 wt% SiO_2 occurring in the Sanak-Baranof belt (SBB). (A) Rocks of the western Sanak-Baranof belt (63–56 Ma). Shaded fields represent previously reported data sets for rocks older than 56 Ma from the western Sanak-Baranof belt. Data sources for these fields are: Kodiak—Ayuso et al. (2009); Sanak-Shumagin—Hill et al. (1981); Seldovia—Lytwyn et al. (2000) and Bradley et al. (2003). Also illustrated are eclogite and garnet amphibolite partial melting curves (labeled 1 and 2, respectively), after Drummond and Defant (1990), which assume a normal mid-ocean-ridge basalt (N-MORB) source (264 ppm Sr, 38 ppm Y). Numbers adjacent to the tick marks indicate degrees of partial melting. (B) Data for rocks of the eastern Sanak-Baranof belt (55–51 Ma) excluding the Crawfish Inlet and Krestof Island plutons. The aqua field represents Cordova samples from the Sheep Bay, McKinley, and Rude River plutons; the aqua star represents a late-stage dacitic dike (Barker et al., 1992). The light-yellow field denotes early-stage intrusions from the Chugach metamorphic complex (CMC), while the yellow stars represent late-stage (Ti_4) postdeformational intrusive dikes established by crosscutting relations (for details, see Harris et al., 1996; Sisson et al., 2003b). The light orange field represents the Mount Draper and Mount Stamy plutons in the Boundary block. The orange star represents a leucogranite that plots off-field (Sisson et al., 2003b). (C) Data for rocks in the far eastern Sanak-Baranof belt (53–47 Ma). The gray field represents adakites (e.g., Drummond and Defant, 1990; Martin, 1999), the blue rectangle represents N-MORB (Gale et al., 2013), and the brown circle represents Chugach–Prince William sediments (Barker et al., 1992; Hill et al., 1981). Symbols are enlarged for samples for which U-Pb ages are available (this study); the smaller symbols lack age data. All enclaves are assumed to be the same age as the host rocks into which they intrude based on field evidence of comagmatic relationships. Note that the Krestof Island host granitoid has an age of 52.1 Ma. The dashed field encompasses younger Crawfish Inlet samples with ages ranging from 51.2 to 47.3 Ma. The gray arrows and tick marks depict the same melting models shown in panel A.

εHf_t compositions ranging from +5.1 ± 0.6 to +7.6 ± 0.3 (Table 2; locations 1, 5, 30, and 32 on Fig. 3). These crystallization ages overlap with each other as well as with those obtained for the Sheep Bay and McKinley Peak plutons, located ~400 km away (Fig. 11A). Mount Draper sample RF16–32A yielded 13 inherited zircons that ranged in age from 1737 to 65 Ma. One sample obtained from the Mount Stamy pluton north of Nunatak Fiord recorded a younger age of 51.4 ± 0.7 Ma, and an εHf_t composition of +6.8 ± 0.5 (Fig. 3, location 19). We also dated a sample (HL19–20) from the Novatak Glacier pluton, which intrudes the Chugach metamorphic complex in the Fairweather Range southeast of Nunatak Fiord; it yielded a crystallization age of 52.0 ± 0.5 Ma. This new concordant age (see Fig. S1) refines the 49 ± 7.3 Ma lower-intercept discordant age reported by Sisson et al. (2003b).

One sample from the Krestof Island pluton north of Sitka recorded an age of 52.5 ± 1.0 Ma and had an εHf_t composition of +10.5 ± 0.5 (Fig. 2). Magmatic zircon from seven samples across the Crawfish Inlet pluton yielded crystallization ages spanning ~6 m.y., from 53.1 ± 0.8 Ma to 47.3 ± 1.2 Ma (Table 2). These Crawfish Inlet samples also displayed a broad range of εHf_t compositions, ranging from +4.7 ± 0.7 to +13.7 ± 0.7 (Fig. 11; Table 2). A muscovite + garnet–bearing leucogranite (CP13–08D) satellite pluton that intrudes the Chugach–Prince William schist adjacent to the composite Crawfish Inlet pluton yielded an age of 52.7 ± 0.8 Ma (Fig. 2).

Our data also suggest that the Crawfish Inlet pluton becomes progressively younger toward its interior. Samples adjacent to intrusive contacts with surrounding country rock recorded ages of 53.1 ± 0.8 Ma (CP13–13) and 52.2 ± 0.9 Ma (CP13–01), respectively. Alternatively, samples collected from the innermost portions of the pluton accessible along the arms of Whale Bay yielded ages of 48.6 ± 1.2 Ma (CP13–03), 48.0 ± 1.0 Ma (CP13–04), and 47.3 ± 1.2 Ma (CP13–09), respectively (Table 2; Fig. 2). This range of ages from the Crawfish Inlet

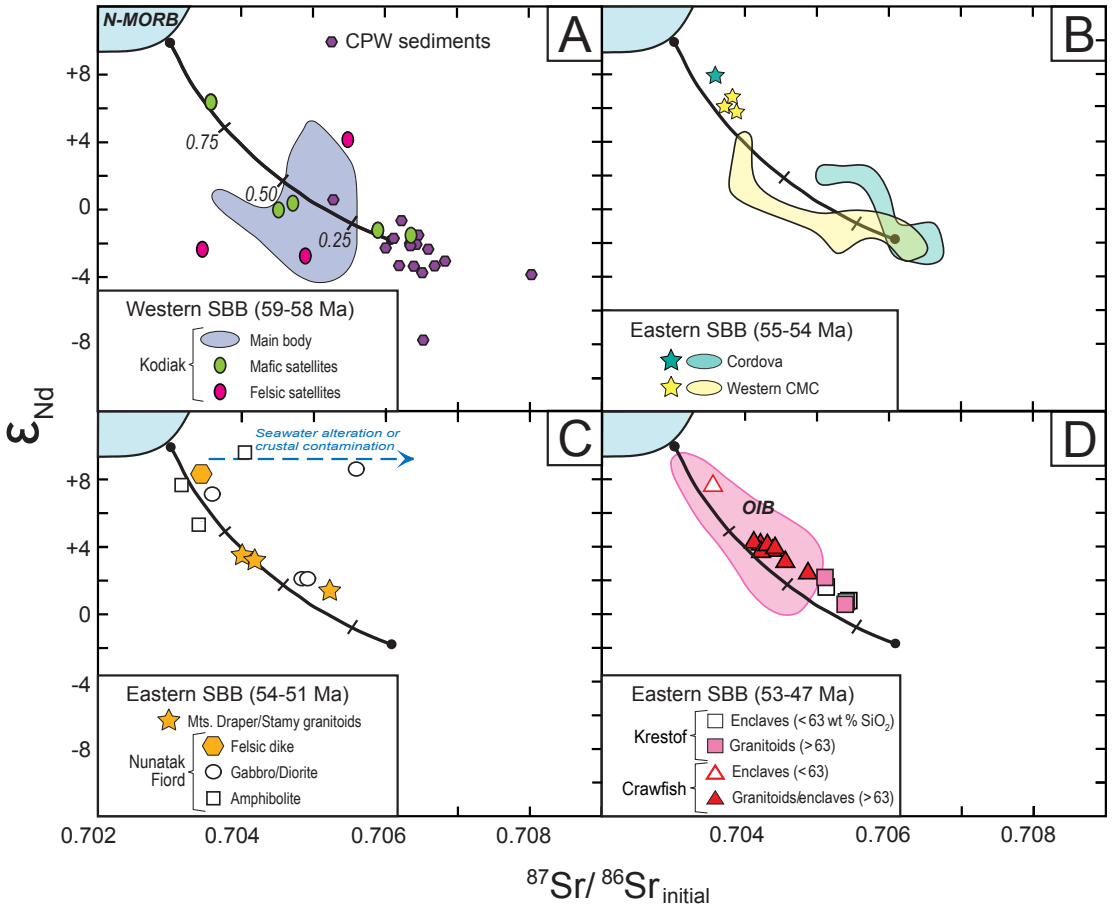

Figure 10. εNd_t vs. $^{87}Sr/^{86}Sr_{initial}$ diagrams for whole-rock samples from this study and other previously published Sr-Nd isotopic data sets for Sanak-Baranof belt (SBB) intrusive rocks. Mixing curves (after Harris et al., 1996) between normal mid-ocean-ridge basalt (N-MORB) and an average Chugach–Prince William (CPW) sedimentary composition are shown in each panel. The numbers next to the tick marks in panel A denote the weight fraction of MORB that was added to sediment in each mixing model. (A) Kodiak batholith samples (data from Ayuso et al., 2009). Also shown are compositions of CPW sedimentary rocks (whole-rock compositions from Farmer et al., 1993, plus one sample from Harris et al., 1996). (B) Intrusive rocks from the Cordova area (Barker et al., 1992) and western Chugach metamorphic complex (CMC; Sisson et al., 2003b). Stars denote late-stage intrusions. (C) Nunatak Fiord and Mount Draper/Stamy samples (Sisson et al., 2003b). Blue dashed arrow is a trend associated with seawater contamination and/or crustal assimilation (Sisson et al., 2003b). (D) Crawfish Inlet and Krestof Island samples (this study). The pink field represents oceanic-island basalts (OIB) after Zindler and Hart (1986), Hofmann (1988, 1997), Sun and McDonough (1989), and Salters and Stracke (2004).

pluton brackets the 51.4 Ma U-Pb age from the Redfish Bay pluton at the southernmost tip of Baranof Island (see Zumsteg et al., 2003).

Detrital Zircon Hf Isotope Compositions

Measured and synthetic Hf isotope data from detrital zircons in Chugach–Prince William turbidites from the Shumagin Islands, Seward, Prince William Sound, Boundary block near Yakutat, and Baranof Island are reported in Table S3. In the Shumagin Islands, the measured εHf_t values ranged from +13.4 to –11.9 (n = 88 zircons), and the probability density plot for the εHf_{50Ma} synthetic data (n = 471) derived from the measured values showed a prominent peak at +8, with an average εHf_{50Ma} value of +2.7 (Fig. 11A). In the Seward area, detrital zircon εHf_t ranged from +15.6 to –12.0 (n = 84) with pronounced peaks at +10 and –5 on a εHf_{50Ma} probability density plot and an average of +0.6 (n = 725). In Prince William Sound, detrital εHf_t spanned a range from +13.5 to –24.4 (n = 184), with a broad εHf_{50Ma} probability density distribution with bookending maxima at +5 and –17 and an average of –5.7 (n = 1484) (Fig. 11A). In the Boundary block, detrital zircon εHf_t values from the schist of Nunatak Fiord ranged from +14.6 to –6.6 (n = 122), with a broad εHf_{50Ma} sawtooth peak from +8 to –4 and an average of +1.8 (n = 590). On Baranof Island, detrital zircon εHf_t values ranged from +9.9 to –15.2 (n = 57), with a broad εHf_{50Ma} peak from +5 to –5 and an average of –1.8 (n = 965) (Fig. 11A).

GEOCHEMICAL TRENDS THROUGH TIME

At the local scale, trace-element and isotopic compositions of the Crawfish Inlet and Krestof

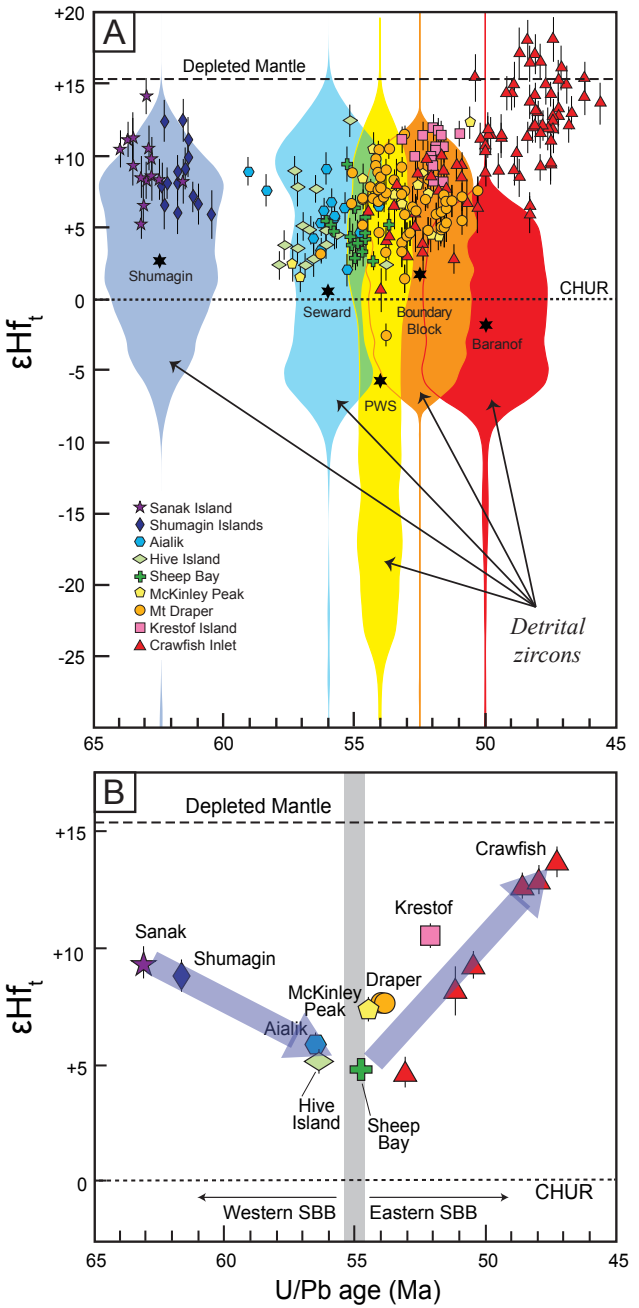

Figure 11. (A) εHf$_t$ values of magmatic zircon from the Sanak-Baranof belt plutons (plotted as symbols) compared with εHf$_{50Ma}$ values for detrital zircon from various Chugach–Prince William turbidite groups (plotted as shaded areas of various colors). Color shaded fields are bubble plots that were constructed from probability density plots of the detrital zircon εHf$_{50Ma}$ data (see Methods and Table S3 [text footnote 2]) and are centered near the U-Pb ages of the intruding plutons. Black stars are the average εHf$_{50Ma}$ values of the detrital zircons. Vertical error bars are ±1σ. CHUR—chondritic uniform reservoir; PWS—Prince William Sound. (B) Weighted means of the εHf$_t$ data from the Sanak-Baranof belt (SBB) plutons. Vertical error bars are ±2σ. Blue arrows highlight the V-shaped time-transgressive trend in εHf$_t$ values for the Sanak-Baranof belt plutons through time.

Island plutons in the far eastern Sanak-Baranof belt change systematically with crystallization age (Fig. 12; Tables 1 and 2; Table S1). Krestof Island and Crawfish Inlet granitoids and evolved (>63 wt% SiO_2) enclaves that are older than 52 Ma all showed lower Sr/Y ratios and are not adakitic (Fig. 9C). With one exception (sample CP13–07A, which was dated at 51.2 Ma), younger (<52 Ma) Crawfish Inlet samples showed Sr/Y characteristics resembling adakites (Fig. 9C). This trend appears to be primarily driven by statistically significant ($P < 0.05$) time-transgressive variations in Y contents (Fig. 12D), which decrease linearly through time ($F_{1,12} = 16.56$; $R^2 = 0.58$; $P = 0.002$). Whole-rock Sr-Nd isotopic compositions of Krestof Island and Crawfish Inlet granitoids also varied through time, becoming more isotopically primitive with decreasing $^{87}Sr/^{86}Sr_{initial}$ ($F_{1,5} = 13.9$; $R^2 = 0.74$; $P = 0.014$; Fig. 12C) and increasing εNd_t ($F_{1,5} = 24.72$; $R^2 = 0.83$; $P = 0.004$; Fig. 12B) values as crystallization age decreases. The time-transgressive variations in bulk-rock elemental and isotopic compositions mirror changes in the average εHf$_t$ values of Crawfish Inlet and Krestof Island magmatic zircon ($F_{1,5} = 21.05$; $R^2 = 0.81$; $P = 0.006$), which also increase with decreasing age (Fig. 12A; Table 2). Complete outputs from the statistical models assessing geochemical variations through time for Krestof Island and Crawfish Inlet magmas are available in Item S1.

Time-transgressive compositional trends in εHf$_t$ are also present at the regional scale across the Sanak-Baranof belt. Whereas differences in analytical methodologies preclude any direct assessment of the relationship between whole-rock geochemical metrics and U-Pb age using previously published data, our systematic collection and analysis of magmatic zircons for both U-Pb age and εHf$_t$ analysis collected from the same sample(s) permitted a robust belt-wide comparative analysis of composition as a function of age across the belt (Fig. 11). During the first period of magmatism, from 63 to 56 Ma, εHf$_t$ values from western Sanak-Baranof belt igneous rocks decrease with decreasing age, reflecting the decline in average εHf$_{50Ma}$ values for the Chugach–Prince William sediments into which they intruded (Fig. 11). During the ensuing 55–47 Ma period, this trend reversed,

and there is a systematic increase in εHf_t values for Sanak-Baranof belt igneous rocks that deviates sharply from the detrital zircon εHf_{50Ma} values for Chugach–Prince William sediments, which are most evolved in the sedimentary rocks exposed in Prince William Sound and on Baranof Island (Fig. 11). Granitoids from the Crawfish Inlet pluton exhibit a linear increase in εHf_t with decreasing age (Fig. 12A) and span a broad compositional range (εHf_t = +4.7 to +13.7).

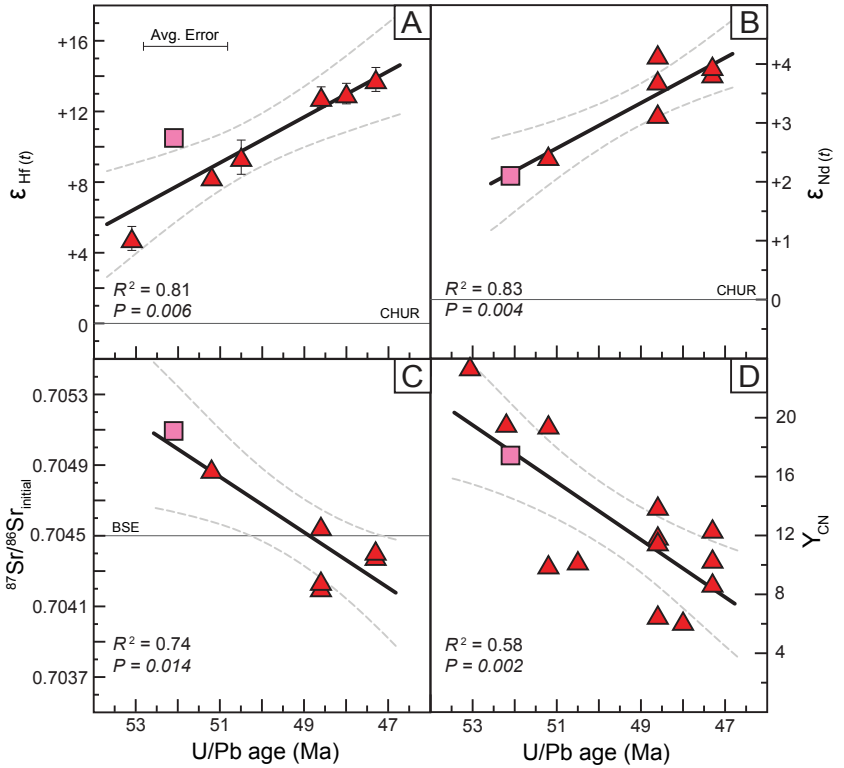

Figure 12. Geochemical trends through time within the Crawfish Inlet (red triangles) and Krestof Island (pink squares) intrusive suites in the far eastern Sanak-Baranof belt. Multiple samples of the same age represent compositions from comagmatic enclaves associated with the host granitoid sample that was U-Pb dated, as in Figure 9. Linear regression fits are shown in black, and the 95% confidence intervals are depicted with light-gray dashed lines. Model goodness-of-fit metrics (i.e., R^2 values) and levels of significance ($P < 0.05$) are also denoted in each panel. (A) Weighted means of the εHf_t data from magmatic zircon vs. U-Pb age (in Ma). Vertical error bars represent ±2σ; some errors are within the symbol size. The line for chondritic uniform reservoir (CHUR) is after Bouvier et al. (2008). (B) Whole-rock εNd_t isotopic compositions vs. U-Pb age (Ma) for Crawfish Inlet and Krestof Island granitoids and evolved (>63 wt%) enclave samples for which both of these metrics are available. The line for CHUR is after Jacobsen and Wasserburg (1980). (C) $^{87}Sr/^{86}Sr_{initial}$ whole-rock compositions vs. U-Pb age (Ma) for Crawfish Inlet and Krestof Island granitoids and evolved (>63 wt%) enclave samples. The line for bulk silicate earth (BSE) at $^{87}Sr/^{86}Sr_{initial}$ = 0.7045 is after Salters and Stracke (2004). (D) Chondrite-normalized Y concentrations (Sun and McDonough, 1989) vs. U-Pb age (Ma) for all Crawfish/Krestof granitoids and enclaves with >63 wt% SiO_2.

DISCUSSION

Geochronological Evidence for the Tale of Two Belts

Early workers recognized that near-trench igneous rocks of the Sanak-Baranof belt record a general time-transgression from west to east, which they ascribed to the migration of a trench-ridge-trench triple junction being subducted obliquely beneath the continental framework (Karig et al., 1976; Marshak and Karig, 1977). Other researchers later refined this trend by expanding the number of dates available for near-trench intrusive rocks across the entire ~2200 km belt, which were found to range from ca. 61 Ma on Sanak Island in the west to ca. 50 Ma on Baranof Island at the belt's eastern edge (Bradley et al., 1993, 2000, 2003; Zumsteg et al., 2003; Farris and Paterson, 2009). On the basis of variably reliable ages for Sanak-Baranof belt intrusive bodies obtained through K/Ar dating of muscovite or biotite (low reliability), $^{40}Ar/^{39}Ar$ dating of muscovite, hornblende, and biotite (intermediate reliability), and U-Pb dating of monazite and magmatic zircon (high reliability), these studies strengthened the case for systematic younging of Sanak-Baranof belt igneous rocks toward the east (Bradley et al., 1993, 2000, 2003). The repeatedly referenced 61–50 Ma age range and systematic younging of Sanak-Baranof belt intrusive suites toward the east have featured prominently in most tectonic reconstructions of the Cordilleran margin—even when the hypothesized tectonic framework models have been at odds. Specific examples of competing tectonic reconstructions that invoke this same systematic temporal trend for Sanak-Baranof belt plutons include the Resurrection plate hypothesis of Haeussler et al. (2003), the Baranof–Leech River hypothesis of Cowan (Cowan, 1982, 2003), and several other Kula and/or Farallon ridge-trench configurations highlighted by Fuston and Wu (2021).

Farris and Paterson (2009) expanded on these previous approaches by applying a linear regression analysis of age as a function of distance from Sanak Island to derive an average estimate for the trench-ridge-trench triple junction migration rate along the margin, which they placed at 19.6 cm yr^{-1}

and leveraged in support of the Resurrection plate hypothesis (Haeussler et al., 2003). However, this presumed linear relationship between Sanak-Baranof belt intrusive age and position along the margin has until now been based on only 12 concordant U-Pb monazite and zircon dates that span the entire ~2200 km of the belt (Bradley et al., 2003; Farris and Paterson, 2009), with half of those available ages coming from the 59–58 Ma Kodiak batholith in the western Sanak-Baranof belt (Farris and Paterson, 2009). Of the remaining six concordant U-Pb ages, only two robust ages had been obtained from the entire eastern half of the belt—a distance of >800 km stretching from the eastern Prince William Sound to Baranof Island (Fig. 1).

We emphasize that it is challenging to reconcile trends in age and composition as a function of position along the modern margin, given the sizeable estimates of northward translation of outboard terranes along the southern Alaskan margin (e.g., Plumley et al., 1983; Bol et al., 1992; Haeussler et al., 2003; Cowan, 2003). Nonetheless, we elected to consider belt-wide trends in this context to allow for direct comparisons with these previous studies of Sanak-Baranof belt rocks. Integration of our new U-Pb crystallization ages ($n = 23$) with existing U-Pb ages from across the belt ($n = 12$; Farris and Paterson, 2009) highlights divergent behavior in eastern Sanak-Baranof belt rocks that deviates from the systematic linear belt-wide relationship reported previously. Running separate linear mixed effects models (see Item S1 for additional discussion and model outputs) for the western and eastern portions of the Sanak-Baranof belt highlighted the finding that distance from Sanak Island explains >97% of the variability in U-Pb crystallization ages for rocks older than 56 Ma in the western Sanak-Baranof belt but only ~51% of the variability in observed U-Pb ages for intrusive rocks younger than 55 Ma in the eastern Sanak-Baranof belt (Fig. 13B). These data collectively suggest that a strong relationship between crystallization age and position along the margin was maintained prior to 57–55 Ma, but this relationship unraveled after ca. 56 Ma.

Our expansion of the available U-Pb age data for igneous rocks across the entire near-trench plutonic belt—and especially within the eastern

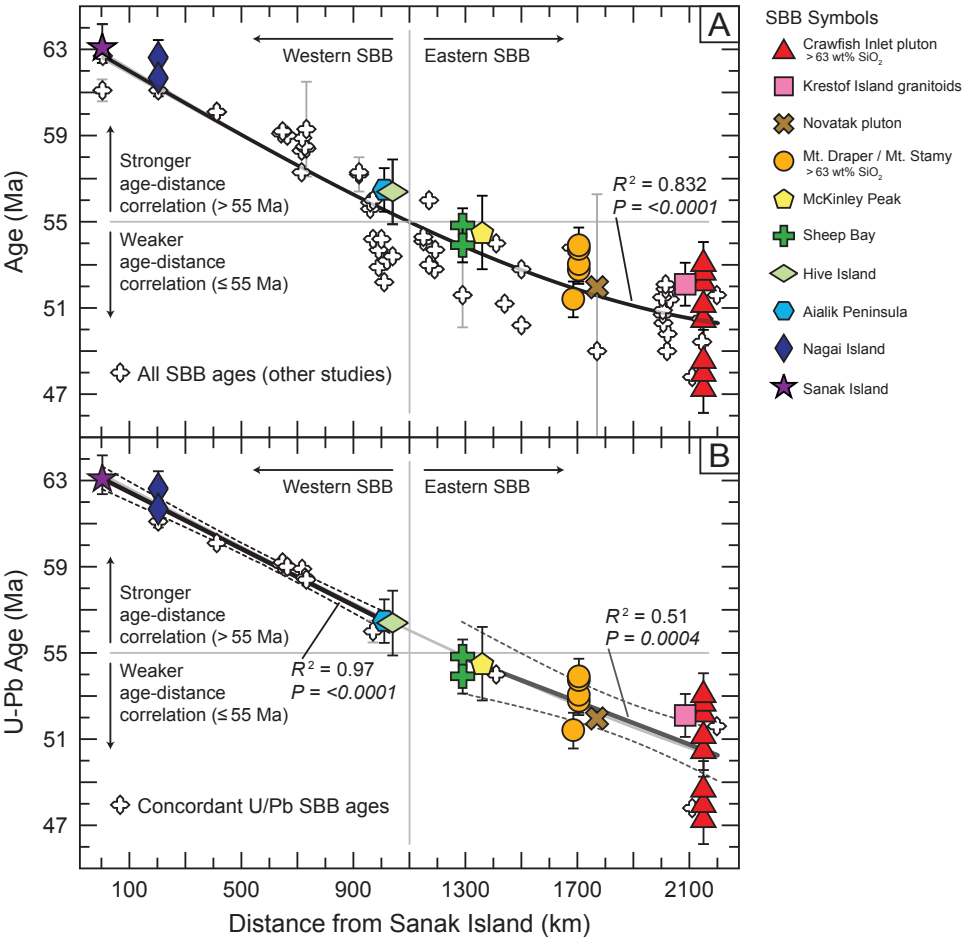

Figure 13. (A) All U-Pb, Ar/Ar, and K/Ar ages from across the Sanak-Baranof belt (SBB), including data from Bradley et al. (1993, 2000, 2003), Haeussler et al. (1995), Sisson et al. (2003b), Zumsteg et al. (2003), and Farris et al. (2006), plotted alongside new concordant U-Pb ages reported here ($n = 23$). White crosses denote previously obtained ages ($n = 54$) from across the belt, while other symbols represent new U-Pb analyses ($n = 23$) from this study, with symbols as shown in Figure 6. The vertical error bars denote standard errors (±2σ) around the mean age. (B) Concordant U-Pb ages for Sanak-Baranof belt intrusive rocks vs. distance (along strike) from Sanak Island (in km). White crosses represent previously obtained ages ($n = 12$; data compiled from Farris and Paterson, 2009). Other symbols represent new analyses ($n = 23$) reported in this study, with symbols as in Figure 6. Vertical error bars denote standard errors (±2σ) around the U-Pb weighted mean ages (see Table 2 for complete U-Pb results from this study).

Sanak-Baranof belt—revealed several key points. First, our new U-Pb zircon ages extend the duration of Sanak-Baranof belt magmatism by almost ~5 m.y. (63–47 Ma) relative to the most commonly cited 61–50 Ma age range, although we note that some studies have alternatively referenced a ca. 61–48 Ma age range for the belt (e.g., Madsen et al., 2006). More importantly, our expanded data set

dispels the long-standing assumption that the age of Sanak-Baranof belt plutons decreases systematically from west to east in relation to position along the modern Alaskan margin, although we also note that Sisson et al. (2003b) did begin to outline the nonlinear age-position relations for Sanak-Baranof belt intrusive rocks within the western Chugach metamorphic complex and Boundary block (i.e., Mount Draper/Stamy plutons).

Our findings build upon the work of Sisson et al. (2003b) and provide a wealth of new geochronological data that portray a more nuanced picture of the timing of early Tertiary near-trench magmatism along the Cordilleran margin, which supports the notion that the Sanak-Baranof belt is better represented as two distinct (i.e., western and eastern) belts (Fig. 13B). Near-trench intrusive rocks emplaced during the first ~7 m.y. of magmatism (from 63 to 56 Ma) record a systematic spatial and temporal relationship, wherein position along the modern-day southern Alaska margin remains a strong predictor of intrusive age. During the second ~9 m.y. of forearc magmatic activity (from 56 to 47 Ma), widespread and long-lived magmatism generated coeval and compositionally heterogeneous near-trench intrusive rocks that are now separated by ~800 km (from Prince William Sound to Baranof Island) along the modern-day margin.

Geochemical Evidence for the Tale of Two Belts

Trace-Element Geochemistry and the Role of Adakites

"Adakite" is the term broadly applied to a class of sodium-rich intrusive and/or extrusive igneous rocks with high Sr/Y ratios, which are compositionally distinct from "normal" mantle wedge-derived arc rocks (Kay, 1978; Drummond and Defant, 1990; Martin, 1999; Martin et al., 2005; Hastie, 2021). Early studies on adakites linked their origin to slab melting (e.g., Drummond and Defant, 1990), but recent work has proposed alternative petrogenetic models for adakite formation (see Hastie, 2021, and references therein). It is now generally recognized that any tectonic environment that involves partial melting of basalt and/or amphibolite at sufficient crustal thicknesses to stabilize garnet and/or amphibole in the residuum can generate adakitic melts (e.g., Beard and Lofgren, 1991; Atherton and Petford, 1993). For example, adakitic melts have been found in intraplate environments stemming from partial melting of delaminated mafic lower crust (Xu et al., 2002). Other researchers have noted that ridge subduction events and the ensuing generation of a "slab window" (Defant et al., 1992; Thorkelson, 1996; Thorkelson and Breitsprecher, 2005) and/or the potential for tearing around the edge of a downgoing slab (Yogodzinski et al., 2001; Thorkelson and Breitsprecher, 2005) constitute tectonic settings commonly associated with adakite formation.

Previous petrogenetic models invoked adakite genesis in the Sanak-Baranof belt by either slab melting (e.g., Haeussler et al., 2003; Sisson et al., 2003b; Farris and Paterson, 2009) and/or partial melting of underplated mafic lower crust (e.g., Harris et al., 1996). Some of these studies also proposed that the Sanak-Baranof belt records systematic differences in Sr/Y ratios along the belt, with lower Sr/Y (non-adakitic) melts in the west that grade toward systematically higher Sr/Y ratios in the eastern Sanak-Baranof belt (e.g., Haeussler et al., 2003; Farris and Paterson, 2009). Farris and Paterson (2009) proposed that higher Sr/Y ratios in the eastern Sanak-Baranof belt are due to the onset of slab melting in this portion of the belt, and they used this line of reasoning to support the Resurrection plate hypothesis of Haeussler et al. (2003).

Our compilation demonstrates that Sr/Y ratios exhibit no clear and consistent trends across the Sanak-Baranof belt (Fig. 9; Item S1). For example, some western Sanak-Baranof belt magmatic systems—namely, the suite of near-trench dikes that intrude the Chugach–Prince William terrane near Seldovia (Kenai Peninsula)—show strongly adakitic Sr/Y ratios (Fig. 9A; Lytwyn et al., 2000; Bradley et al., 2003). These compositionally heterogeneous dikes have been dated to 57.0 ± 0.2 Ma by $^{39}Ar/^{40}Ar$ methods (Bradley et al., 2000), consistent with interpretations that they form part of the Sanak-Baranof belt (Lytwyn et al., 2000; Bradley et al., 2003). The Seldovia dikes have high Sr/Y ratios (Fig. 9A; Item S1; Lytwyn et al., 2000; Bradley et al., 2003) with values up to 175 (plotting off scale in Fig. 9A), despite lying ~300–400 km west of the definitively non-adakitic ca. 55 Ma Sheep Bay, Rude River, and McKinley Peak plutons exposed near Cordova (Fig. 9B; this study; Barker et al., 1992).

Many eastern Sanak-Baranof belt suites also show extremely variable Sr/Y ratios and Y contents. The largest range is observed for granitoids from the Mount Draper and Mount Stamy plutons, with Sr/Y values approaching ~200–225 (plotting off scale in Fig. 9B). The sparse U-Pb ages we obtained for these rocks did not reveal any temporal trends in Sr/Y. The Crawfish Inlet rocks exhibited a moderate range of Sr/Y ratios (~9–55), some of which overlap with the adakite field (Fig. 9C). Our detailed geochronology for this pluton highlighted a trend toward increasing Sr/Y through time (Fig. 12). This trend of increasing Sr/Y through time appears to be consistent for both the Crawfish Inlet and several other eastern Sanak-Baranof belt suites, as late-stage dikes in both the Cordova area (Fig. 9B; Barker et al., 1992) and western Chugach metamorphic complex (Fig. 9B; Harris et al., 1996; Sisson et al., 2003b) are notably more adakitic than earlier intrusive units within these suites. However, more detailed age dating is needed to confirm this trend more reliably within other eastern Sanak-Baranof belt suites.

The lack of systematic variations in Sr/Y ratios across the Sanak-Baranof belt (Fig. 9; Item S1) challenges the notion that adakitic "slab melts" are largely confined to younger rocks in the eastern Sanak-Baranof belt (e.g., Haeussler et al., 2003; Farris and Paterson, 2009). Besides slab melting and/or melting of mafic crust, there are several other possible explanations for the development of highly variable Sr/Y ratios within individual Sanak-Baranof belt intrusive suites. One recent review (Luffi and Ducea, 2022, and references therein) considered the use of whole-rock geochemical parameters that correlate with crustal thickness (i.e., "mohometers"). They proposed Sr/Y ratios as one of the metrics that best serves as a qualitative proxy of paleo-Moho depths. In line with this work, one possible explanation for the observed increase in Sr/Y through time in the Crawfish Inlet

suite could be increasing crustal thickness during petrogenesis, leading to melting at greater depths and pressures that stabilized garnet in the residuum. Although the Crawfish Inlet pluton could be anomalous, this mechanism for adakite genesis seems to be somewhat unlikely given the wealth of evidence for extensive plutonism associated with transtension in other portions of the eastern Sanak-Baranof belt ca. 55–50 Ma (e.g., Sisson and Pavlis, 1993; Pavlis and Sisson, 2003; Gasser et al., 2011).

Another mechanism capable of generating high Sr/Y ratios while lowering Y contents is fractionation of minerals with high distribution coefficients for Y but low coefficients for Sr. Examples of such phases include hornblende, garnet, zircon, and titanite (Sisson and Bacon, 1992; Ewart and Griffin, 1994; Bachmann et al., 2005; Ackerson, 2011; Padilla and Gualda, 2016). Both zircon and garnet have high distribution coefficients for Y (~130–180) and very low distribution coefficients for Sr (<0.02). Thus, removal of ~2%–3% garnet and/or zircon would result in rapid depletion of Y and a concomitant increase in Sr/Y ratios (>20-fold). The Sr distribution coefficients are similar for hornblende and titanite (average ~0.5–0.6), but the Y distribution coefficient for titanite (~720) is enormous compared to that for hornblende (~14). Removal of as little as 0.02% titanite could drastically deplete Y and increase Sr/Y ratios to >10,000. In contrast, fractionation of ~15% hornblende would increase initial values of Sr/Y from ~10 up to ~95 and decrease initial values of Y from ~25 to <5, consistent with the variations observed for Crawfish Inlet granitoids (Fig. 9C). In other words, increases in Sr/Y in younger Crawfish Inlet magmas (and potentially other eastern Sanak-Baranof belt suites) could also stem from fractionation processes rather than deeper melting and/or variable involvement of partially melted mafic crust.

Although our belt-wide Sr/Y compilation challenges previous assertions that the western and eastern portions of the Sanak-Baranof belt can be distinguished by the presence (or absence) of adakites, we do build upon the premise originally introduced by Farris and Paterson (2009), who stated that intrusive rocks from the western and eastern belts are systematically different. We propose instead that this tale of two belts is best illuminated by whole-rock Sr/Nd isotopes and particularly by εHf_t analyses of magmatic zircon, rather than through Sr/Y dynamics or other trace-element characteristics. The increasing εHf_t and Sr/Nd isotopic signatures through time across much of the eastern Sanak-Baranof belt may reflect a greater involvement of isotopically primitive source end members, which could also have contributed to the temporal trends in Sr/Y we observed within many of the eastern Sanak-Baranof belt suites.

Sr and Nd Isotopic Constraints

Our data set from the Crawfish Inlet pluton documents systematic, time-transgressive compositional Sr-Nd isotopic variations recorded through time (~6 m.y.) within an individual pluton (Fig. 12; Item S1). There are many other well-studied examples of systematic age and geochemical variations within individual intrusive suites. For example, significant age ranges (from ~3 to 19 m.y.) have been documented in temporally and chemically zoned plutons of the Sierra Nevada batholith (e.g., Bateman, 1992; Coleman et al., 2004; Davis et al., 2012; Lackey et al., 2012; Putnam et al., 2015), as well as plutons of the Aleutian (e.g., Kay et al., 2019) and Andean arcs (González Guillot et al., 2018; Rodríguez et al., 2019).

We suggest that this local signature of increasing mantle-derived proportions through time may comprise a characteristic signature across much of the eastern Sanak-Baranof intrusive belt (the Boundary block notwithstanding) and that this time-transgressive signature may in turn be used to distinguish between the western and eastern belts. Future studies may aim to better constrain the temporal and compositional relations at local levels within the Cordova, western Chugach metamorphic complex, and Yakutat area (Boundary block) intrusive suites to further test this assumption. Furthermore, higher-resolution sampling and detailed characterization of near-trench igneous activity at local scales (i.e., within individual plutons and/or plutonic suites) across other tectonic environments that have recorded ridge-trench encounters, such as in Japan (Maeda and Kagami, 1996; Shinjoe et al., 2021) and/or Patagonia (e.g., Forsythe et al., 1986; D'Orazio et al., 2000; Lagabrielle et al., 2000), may illuminate whether this trend is a recurring pattern associated with forearc slab window magmatism more generally or whether it is unique to the eastern portions of the Sanak-Baranof belt.

Hf Isotopic Constraints

Arguably the clearest case for partitioning the Sanak-Baranof belt into two separate belts is illustrated by our belt-wide compilation of εHf_t values versus U-Pb age (Ma) for the Sanak-Baranof belt plutons (Fig. 11). In the western belt, εHf_t values of the plutons become systematically more evolved from west to east, and they appear to track with the εHf_{50Ma} signatures of the sedimentary rocks into which they intrude (Fig. 11A). This finding supports a model of petrogenesis via mixing between depleted mantle melts and assimilation of Chugach–Prince William sedimentary rocks (e.g., Hill et al., 1981; Barker et al., 1992; Ayuso et al., 2009). In contrast, the εHf_t of the oldest plutons in the eastern belt (54 Ma) are the most evolved and become systematically more primitive with decreasing age (Fig. 11).

The consistent lowering of εHf_t values in western Sanak-Baranof belt rocks from Sanak Island to Prince William Sound could reflect an increase in the amount of assimilation of sedimentary rocks by N-MORB mantle melts toward the east. Barker et al. (1992) suggested Chugach–Prince William sedimentary proportions may be as high as ~90% in some Cordova area plutons, and the presence of kyanite xenocrysts in some western Sanak-Baranof belt granitoids like the Aialik and Nuka plutons (e.g., Kusky et al., 2003) further implicates a substantial metasedimentary contribution to Sanak-Baranof belt melts near the western-eastern transition zone. However, we also highlight the possibility that the lower εHf_t of Cordova area plutons could alternatively reflect a compositional shift toward a lower εHf_{50Ma} signature for the Chugach–Prince William sedimentary rocks around Prince William Sound (Fig. 11). On Baranof Island, the average εHf_{50Ma} of

the Sitka Graywacke and Baranof schist is –1.8, and the εHf_t value of the oldest sample of the Crawfish Inlet pluton (53 Ma) is +4.7 (Fig. 11; Table 2). Therefore, the increase in εHf_t toward more primitive values with age in the Crawfish Inlet pluton (as high as +13.7 at 47 Ma) likely reflects greater proportions of mantle-derived melts with time, consistent with the time-transgressive trends in Sr-Nd isotopic and trace-elemental compositions (Fig. 12).

One possible explanation for the increasing mantle component over the ~6 m.y. of magmatism in the Crawfish Inlet pluton is that there was a "clearing out" of the magmatic plumbing system during this long-lived magmatic episode, with a concomitant decrease in sediment assimilation through time. Within this framework, shorter-lived magmatism (~1–2 m.y.; see Farris and Paterson, 2009) within the western Sanak-Baranof belt does not record this transition, causing the εHf_t isotopic signatures of the western Sanak-Baranof belt plutons to track more closely with those of the sediments into which they intrude. Potential tectonic frameworks that explicitly link to the increasing mantle contributions in eastern Sanak-Baranof belt rocks could include: (1) an increasing mantle end-member component that was supplemented by interactions between the more southerly paleo–Chugach–Prince William terrane and ancestral Yellowstone hotspot (Wells et al., 2014), which would also help to explain the additional heat source necessary to generate the observed metamorphic assemblages on southern Baranof Island (see Zumsteg et al., 2003), and/or (2) protracted transtensional activity in the ancient forearc during plate reorganization, which in turn facilitated partial melting of the mafic rocks that are interbedded with younger Chugach–Prince William sediments (Sisson and Pavlis, 1993; Pavlis and Sisson, 2003; Gasser et al., 2011).

SUMMARY AND CONCLUSIONS

The time-transgressive Sanak-Baranof belt exposed over ~2200 km along the southern margin of Alaska may be a tale of two belts: (1) a western belt with crystallization ages that become younger systematically from 63 Ma in the west (Sanak Island) to 56 Ma in the east (Resurrection Bay) and (2) an eastern belt with broadly coeval crystallization ages ranging from 55 to 47 Ma that spans >800 km along strike from eastern Prince William Sound to Baranof Island (Table 2; Fig. 1). Major- and trace-element geochemistry and petrography of Sanak-Baranof belt intrusive rocks show that they vary widely in composition and classification, from gabbros to garnet + muscovite–bearing leucogranites. Whole-rock elemental and isotopic observations fail to clearly elucidate systematic differences between the western and eastern belts, including Sr/Y ratios and Sr-Nd isotopic values (Figs. 9 and 10). In the western belt, εHf_t values of magmatic zircon from the Sanak-Baranof belt plutons vary from +9.3 ± 0.7 on Sanak Island to +5.1 ± 0.5 at Resurrection Bay, and this trend tracks the decreasing εHf_{50Ma} signature of detrital zircons from the Chugach–Prince William turbidites into which they intrude (Fig. 11). In the eastern belt, there is a distinct and systematic departure of εHf_t values for the plutons compared to the εHf_{50Ma} values recorded by the surrounding Chugach–Prince William turbidites. This is particularly pronounced at the easternmost edge of the belt on Baranof Island, where the Chugach–Prince William turbidites have an average $\varepsilon Hf_{50Ma} = -1.8$, while the oldest phases of the Crawfish Inlet pluton (ca. 53 Ma) have $\varepsilon Hf_t = +4.7$ and the youngest phases (47 Ma) have $\varepsilon Hf_t = +13.7$, which approaches the εHf_t value for depleted mantle (Fig. 11).

These new observations and syntheses, spanning the entire ~2200 km of the Sanak-Baranof belt, suggest that this is a tale of two belts composed of a wide variety of granitoid rocks, which precludes a simple time-transgressive emplacement of plutons along the Paleocene–Eocene Alaskan margin due to sweeping subduction of a migrating ridge. Most plate reconstructions for the NE Pacific Basin indicate that emplacement of the Sanak-Baranof belt plutons occurred in a strike-slip environment that resulted in northward translation along the Cordilleran margin following intrusion, but the relationship to offshore plate geometries remains unclear because offshore marine magnetic anomalies of that age have long since been subducted (Engebretson et al., 1985; Shephard et al., 2013; Müller et al., 2019; Clennett et al., 2020; Fuston and Wu, 2021). Several observations highlight the tectonic complexity and unique attributes of the eastern Sanak-Baranof belt, which distinguishes this portion of the belt from >56–55 Ma Sanak-Baranof belt plutons situated to the west.

First, intrusion of eastern Sanak-Baranof belt rocks likely occurred in a dextral strike-slip environment that was in part manifested by significant slip on the Border Ranges fault system. For example, the Tarr Inlet suture of the Border Ranges fault system appears to have hundreds of kilometers of dextral slip (up to ~700 km) that occurred between 58 Ma and 42 Ma (Smart et al., 1996; Sisson et al., 2003b). Strike-slip faults are also common within rocks of the Chugach–Prince William terrane and are especially apparent across the eastern Sanak-Baranof belt, where several structures appear to have accommodated particularly significant movement between the late Paleocene and early to middle Eocene (Bol and Roeske, 1993).

Second, wholesale crustal stretching and extension likely accompanied eastern Sanak-Baranof belt plutonism, and extension-derived "bimodal" igneous products offer an intriguing explanation for the apparent compositional gap in SiO_2 contents for (eastern) Sanak-Baranof belt intrusive rocks (see Figs. 6 and 7). The Chugach metamorphic complex in the eastern Chugach Range records a remarkable sequence of synchronous plutonism and transtension between ca. 55 Ma and 50 Ma (see Sisson and Pavlis, 1993; Pavlis and Sisson, 2003; Gasser et al., 2011). The 57 Ma Resurrection ophiolite and its allied fragments may have also resulted from extreme transtension in the upper plate (Davidson and Garver, 2017). These observations suggest crustal thickening was likely not responsible for the observed increase in Sr/Y ratios through time for many (but not all) eastern Sanak-Baranof belt suites.

Third, although the offshore plate setting remains poorly understood, many tectonic models call upon interactions with an offshore ridge at a triple junction. To explain the geologic complexity of the (eastern) Sanak-Baranof belt, Sisson and Pavlis (1993) proposed that the subduction of transform offsets from a spreading ridge may have allowed certain areas along the margin to

experience prolonged heating and/or repeated reheating (see Sisson and Pavlis, 1993; Pavlis and Sisson, 2003). Ridge segments and transforms may have therefore been juxtaposed at steep angles relative to the margin, with some segments subducting obliquely or nearly parallel to the margin (Sisson et al., 2003b). Eastern Sanak-Baranof belt magmas were thus likely affected by complexities in the nature of the offshore spreading ridge, which may have assumed enigmatic orientations and/or behavior during the dynamic period of plate reconfiguration between 56 Ma and 52 Ma (Sisson and Pavlis, 1993).

Last, paleomagnetic results from rocks of the Chugach–Prince William terrane (host to the Sanak-Baranof belt) raise the possibility that intrusion occurred far to the south, and the Chugach–Prince William terrane and Sanak-Baranof belt were subsequently translated northward to Alaska. The available paleomagnetic data indicate ~1400–2500 km of margin-parallel translation of the 57 Ma Resurrection Peninsula ophiolite and slightly older rocks on Kodiak Island (for further discussion, see Garver and Davidson, 2015). Published models suggest the age distribution of Sanak-Baranof belt plutons may be related to either movement of offshore plate geometries (see Clennett et al., 2020; Fuston and Wu, 2021) and/or movement of the Chugach–Prince William terrane as a strike-slip–bound forearc sliver (or possibly both). In any case, the enigmatic nature of the eastern Sanak-Baranof belt is almost certainly related to the complexity of the dynamic Pacific plate reorganizations that occurred around chron 24–23 (between ca. 56 Ma and 52 Ma; Pavlis and Sisson, 1995; Wells et al., 2014; Clennett et al., 2020; Fuston and Wu, 2021).

The original tectonic setting of the Sanak-Baranof belt and coeval plutonism in the Pacific Northwest (e.g., Madsen et al., 2006; Wells et al., 2014) are a Cordilleran conundrum. On the one hand, the timing and spatial distribution of the Sanak-Baranof belt have been used to infer an in situ setting wherein near-trench plutonism was driven by subduction and spreading of the now-vanished hypothetical Resurrection plate. This tectonic framework requires rejection of numerous paleomagnetic data sets that show the host rocks to the Sanak-Baranof belt have shallow inclinations and thus were formed much farther south along the Cordilleran margin. On the other hand, an ex situ or far-traveling scenario—which honors the paleomagnetic data—requires a complex petro-tectonic scenario where intrusion and concurrent strike-slip faulting carried the Sanak-Baranof belt plutons and Chugach–Prince William terrane over a thousand kilometers northward.

This latter hypothesis is further complicated by the fact that the original position of intrusion may have also overlapped with the ancestral Yellowstone hotspot (Wells et al., 2014), which could have generated additional melting in an oblique subduction setting, wherein end-member oceanic-island basalt chemistry would likely be substantially modified by subduction zone processes. Regardless, excision of these rocks and translation along the margin would have left a truncation scar, which some have recognized (i.e., Johnson, 1984). These two hypotheses—in situ and ex situ—are mutually exclusive, and we are left with two separate options: Either the Sanak-Baranof belt plutons intruded the Chugach–Prince William terrane more or less in place (i.e., Alaska) or they were intruded far to the south and subsequently translated northward. There is no middle ground. The conundrum is that although these near-trench plutons should be ideal contenders to help constrain the offshore plate setting, they cannot help to clarify Cordilleran tectonic reconstructions until their original site of intrusion is resolved. One thing seems clear: The Sanak-Baranof belt records a transition at ca. 57–55 Ma, which likely reflects a dynamic period of plate reorganization in the North Pacific Basin.

It is beyond the scope of this study to parse the potential mechanisms and tectonic scenarios that comprehensively address all the available geochemical, geochronological, structural, and paleomagnetic data. However, some viable possibilities seem to include a combination of oblique ridge subduction interacting with a dynamic transpressional to transtensional margin, which was simultaneously undergoing rapid sedimentation and tectonic thickening in the forearc stemming from exhumation and erosion of the Coast plutonic complex (Hollister, 1979; Haeussler et al., 2006; Davidson and Garver, 2017). In the easternmost Sanak-Baranof belt, these events may have also been facilitated and/or followed by interactions with the ancestral Yellowstone hotspot (e.g., Wells et al., 2014) and ensuing dextral strike-slip transport along the margin, which carried both the Chugach–Prince William and Yakutat terranes northward to their modern-day position in southern Alaska. Regardless of what tectonic mechanisms are invoked, our findings clarify (at local scales) and complicate (at regional scales) the current picture of geochemical and geochronological relations across the Sanak-Baranof belt, and these results must be accounted for in future tectonic reconstructions of the Paleocene–Eocene Cordilleran margin.

ACKNOWLEDGMENTS

We are grateful to: Staci Loewy at the University of Texas–Austin Isotope Geochemistry laboratory for elemental and isotope analyses, Washington State University GeoAnalytical laboratory for major- and trace-element analyses, and the Arizona LaserChron Center for U-Pb and Hf analyses of magmatic and detrital zircon. We are indebted to a number of students over the years who have worked on the broader project across southern Alaska, including Brianna Rick, Brian Frett, Kate Kaminski, Meghan Riehl, Claudia Roig, Erin Arntson, Rainer Lempert, and Alex Short, who all contributed discussions, fieldwork, and myriad analyses as part of their thesis research. We have had fruitful discussions in the field with Darrel Cowan, Peter Crowley, and Eva Enkelmann. We also thank Virginia Sisson, Erin Todd, and Eric H. Christiansen for their thoughtful reviews and suggestions, which greatly improved the manuscript. This work was supported by National Science Foundation grants EAR-1116554 and EAR-1728013 to J.I. Garver and EAR-1116536 and EAR-1727991 to C.M. Davidson. This work was also partially funded by Keck Geology Consortium and Semmes Distinguished Science fellowships awarded to A.A. Wackett from Trinity University, as well as National Science Foundation Graduate Research Fellowship grant DGE-2146755 to Wackett. D.R. Smith also thanks Trinity University for providing Herndon Professorship and faculty development funds, which further supported this work.

REFERENCES CITED

Ackerson, M.R., 2011, Trace Element Partitioning Between Titanite and Groundmass in Silicic Volcanic Systems [M.S. thesis]: Chapel Hill, North Carolina, University of North Carolina at Chapel Hill, 76 p.

Arntson, E., 2018, U-Pb Ages and Hf Isotope Composition of the Mt. Draper and Mt. Stamy Plutons, Nunatak Fjord, Alaska: Implications for the Sanak-Baranof Plutonic Belt [B.A. thesis]: Northfield, Minnesota, Carleton College, 68 p.

Arntson, E., Olson, H., Davidson, C., and Garver, J.I., 2017, Geochemistry, U-Pb ages, and Hf isotopes of the Mt. Draper

and Mt. Stamy plutons, Nunatak Fjord, Alaska: Implications for the Sanak-Baranof plutonic belt: Geological Society of America Abstracts with Programs, v. 49, https://doi.org/10.1130/abs/2017CD-292866.

Atherton, M.P., and Petford, N., 1993, Generation of sodium-rich magmas from newly underplated basaltic crust: Nature, v. 362, p. 144–146, https://doi.org/10.1038/362144a0.

Ayuso, R.A., Haeussler, P.J., Bradley, D.C., Farris, D.W., Foley, N.K., and Wandless, G.A., 2009, The role of ridge subduction in determining the geochemistry and Nd-Sr-Pb isotopic evolution of the Kodiak batholith in southern Alaska: Tectonophysics, v. 464, p. 137–163, https://doi.org/10.1016/j.tecto.2008.09.029.

Bachmann, O., Dungan, M.A., and Bussy, F., 2005, Insights into shallow magmatic processes in large silicic magma bodies: The trace element record in the Fish Canyon magma body, Colorado: Contributions to Mineralogy and Petrology, v. 149, p. 338–349, https://doi.org/10.1007/s00410-005-0653-z.

Barker, F., 1979, Trondhjemite: Definition, environment and hypotheses of origin, *in* Barker, F., ed., Trondhjemites, Dacites, and Related Rocks: Amsterdam, Netherlands, Elsevier, Developments in Petrology 6, p. 1–12, https://doi.org/10.1016/B978-0-444-41765-7.50006-X.

Barker, F., Farmer, G.L., Ayuso, R.A., Plafker, G., and Lull, J.S., 1992, The 50 Ma granodiorite of the eastern Gulf of Alaska: Melting in an accretionary prism in the forearc: Journal of Geophysical Research: Solid Earth, v. 97, p. 6757–6778, https://doi.org/10.1029/92JB00257.

Bateman, P.C., 1992, Plutonism in the Central Part of the Sierra Nevada Batholith, California: U.S. Geological Survey Professional Paper 1483, 186 p., https://doi.org/10.3133/pp1483.

Beard, J.S., and Lofgren, G.E., 1991, Dehydration melting and water-saturated melting of basaltic and andesitic greenstones and amphibolites at 1, 3, and 6.9 kb: Journal of Petrology, v. 32, p. 365–401, https://doi.org/10.1093/petrology/32.2.365.

Bol, A.J., and Roeske, S.M., 1993, Strike-slip faulting and block rotation along the contact fault system, eastern Prince William Sound, Alaska: Tectonics, v. 12, p. 49–62, https://doi.org/10.1029/92TC01324.

Bol, A.J., Coe, R.S., Grommé, C.S., and Hillhouse, J.W., 1992, Paleomagnetism of the Resurrection Peninsula, Alaska: Implications for the tectonics of southern Alaska and the Kula-Farallon Ridge: Journal of Geophysical Research: Solid Earth, v. 97, p. 17,213–17,232, https://doi.org/10.1029/92JB01292.

Bouvier, A., Vervoort, J.D., and Patchett, P.J., 2008, The Lu-Hf and Sm-Nd isotopic composition of CHUR: Constraints from unequilibrated chondrites and implications for the bulk composition of terrestrial planets: Earth and Planetary Science Letters, v. 273, p. 48–57, https://doi.org/10.1016/j.epsl.2008.06.010.

Bradley, D.C., Haeussler, P.J., and Kusky, T.M., 1993, Timing of Early Tertiary Ridge Subduction in Southern Alaska: A Section in Geologic Studies in Alaska by the U.S. Geological Survey, 1992: U.S. Geological Survey Bulletin 2068, 15 p., https://doi.org/10.3133/70180223.

Bradley, D.C., Parrish, R., Clendenen, W., Lux, D.R., Layer, P.W., Heizler, M., and Donley, D.T., 2000, New Geochronological Evidence for the Timing of Early Tertiary Ridge Subduction in Southern Alaska: A Section in Geologic Studies in Alaska by the U.S. Geological Survey, 1998: U.S. Geological Survey Professional Paper 1615, 17 p., https://doi.org/10.3133/70180636.

Bradley, D.C., Kusky, T.M., Haeussler, P.J., Goldfarb, R.J., Miller, M.L., Dumoulin, J.A., Nelson, S.W., and Karl, S.M., 2003, Geologic signature of early Tertiary ridge subduction in Alaska, *in* Sisson, V.B., Roeske, S.M., and Pavlis, T.L., eds., Geology of a Transpressional Orogen Developed during Ridge-Trench Interaction along the North Pacific Margin: Geological Society of America Special Paper 371, p. 19–49, https://doi.org/10.1130/0-8137-2371-X.19.

Bruand, E., Gasser, D., Bonnand, P., and Stuewe, K., 2011, The petrology and geochemistry of a metabasite belt along the southern margin of Alaska: Lithos, v. 127, p. 282–297, https://doi.org/10.1016/j.lithos.2011.07.026.

Bruand, E., Gasser, D., and Stüwe, K., 2014, Metamorphic *P-T* conditions across the Chugach metamorphic complex (Alaska)—A record of focussed exhumation during transpression: Lithos, v. 190–191, p. 292–312, https://doi.org/10.1016/j.lithos.2013.12.007.

Carr, M.J., and Gazel, E., 2017, Igpet software for modeling igneous processes: Examples of application using the open educational version: Mineralogy and Petrology, v. 111, p. 283–289, https://doi.org/10.1007/s00710-016-0473-z.

Clennett, E.J., Sigloch, K., Mihalynuk, M.G., Seton, M., Henderson, M.A., Hosseini, K., Mohammadzaheri, A., Johnston, S.T., and Müller, R.D., 2020, A quantitative tomotectonic plate reconstruction of western North America and the eastern Pacific Basin: Geochemistry, Geophysics, Geosystems, v. 21, https://doi.org/10.1029/2020GC009117.

Coleman, D.S., Gray, W., and Glazner, A.F., 2004, Rethinking the emplacement and evolution of zoned plutons: Geochronologic evidence for incremental assembly of the Tuolumne intrusive suite, California: Geology, v. 32, p. 433–436, https://doi.org/10.1130/G20220.1.

Colpron, M., Nelson, J.L., and Murphy, D.C., 2007, Northern Cordilleran terranes and their interactions through time: GSA Today, v. 17, no. 4/5, p. 4–10, https://doi.org/10.1130/GSAT01704-5A.1.

Cowan, D.S., 1982, Geological evidence for post–40 m.y. B.P. large-scale northwestward displacement of part of southeastern Alaska: Geology, v. 10, p. 309–313, https://doi.org/10.1130/0091-7613(1982)10<309:GEFPMB>2.0.CO;2.

Cowan, D.S., 2003, Revisiting the Baranof–Leech River hypothesis for early Tertiary coastwise transport of the Chugach–Prince William terrane: Earth and Planetary Science Letters, v. 213, p. 463–475, https://doi.org/10.1016/S0012-821X(03)00300-5.

Davidson, C., and Garver, J.I., 2017, Age and origin of the Resurrection ophiolite and associated turbidites of the Chugach–Prince William terrane, Kenai Peninsula, Alaska: The Journal of Geology, v. 125, p. 681–700, https://doi.org/10.1086/693926.

Davis, J.W., Coleman, D.S., Gracely, J.T., Gaschnig, R., and Stearns, M., 2012, Magma accumulation rates and thermal histories of plutons of the Sierra Nevada batholith, CA: Contributions to Mineralogy and Petrology, v. 163, p. 449–465, https://doi.org/10.1007/s00410-011-0683-7.

Defant, M.J., Jackson, T.E., Drummond, M.S., de Boer, J.Z., Bellon, H., Feigenson, M.D., Maury, R.C., and Stewart, R.H., 1992, The geochemistry of young volcanism throughout western Panama and southeastern Costa Rica: An overview: Journal of the Geological Society, v. 149, p. 569–579, https://doi.org/10.1144/gsjgs.149.4.0569.

Didier, J., 1973, Granites and Their Enclaves: The Bearing of Enclaves on the Origin of Granites: Amsterdam, Netherlands, Elsevier, Developments in Petrology 3, 393 p.

D'Orazio, M., Agostini, S., Mazzarini, F., Innocenti, F., Manetti, P., Haller, M.J., and Lahsen, A., 2000, The Pali Aike volcanic field, Patagonia: Slab-window magmatism near the tip of South America: Tectonophysics, v. 321, p. 407–427, https://doi.org/10.1016/S0040-1951(00)00082-2.

Drummond, M.S., and Defant, M.J., 1990, A model for trondhjemite-tonalite-dacite genesis and crustal growth via slab melting: Archean to modern comparisons: Journal of Geophysical Research: Solid Earth, v. 95, p. 21,503–21,521, https://doi.org/10.1029/JB095iB13p21503.

Dumoulin, J.A., 1988, Sandstone petrographic evidence and the Chugach–Prince, William terrane boundary in southern Alaska: Geology, v. 16, p. 456–460, https://doi.org/10.1130/0091-7613(1988)016<0456:SPEATC>2.3.CO;2.

Engebretson, D.C., Cox, A., and Gordon, R.G., 1985, Relative Motions Between Oceanic and Continental Plates in the Pacific Basin: Geological Society of America Special Paper 206, 59 p., https://doi.org/10.1130/SPE206-p1.

Ewart, A., and Griffin, W.L., 1994, Application of proton-microprobe data to trace-element partitioning in volcanic rocks: Chemical Geology, v. 117, p. 251–284, https://doi.org/10.1016/0009-2541(94)90131-7.

Farmer, G.L., Ayuso, R., and Plafker, G., 1993, A Coast Mountains provenance for the Valdez and Orca groups, southern Alaska, based on Nd, Sr, and Pb isotopic evidence: Earth and Planetary Science Letters, v. 116, p. 9–21, https://doi.org/10.1016/0012-821X(93)90042-8.

Farris, D.W., and Paterson, S.R., 2009, Subduction of a segmented ridge along a curved continental margin: Variations between the western and eastern Sanak-Baranof belt, southern Alaska: Tectonophysics, v. 464, p. 100–117, https://doi.org/10.1016/j.tecto.2007.10.008.

Farris, D.W., Haeussler, P., Friedman, R., Paterson, S.R., Saltus, R.W., and Ayuso, R., 2006, Emplacement of the Kodiak batholith and slab-window migration: Geological Society of America Bulletin, v. 118, p. 1360–1376, https://doi.org/10.1130/B25718.1.

Forsythe, R.D., Nelson, E.P., Carr, M.J., Kaeding, M.E., Herve, M., Mpodozis, C., Soffia, J.M., and Harambour, S., 1986, Pliocene near-trench magmatism in southern Chile: A possible manifestation of ridge collision: Geology, v. 14, p. 23–27, https://doi.org/10.1130/0091-7613(1986)14<23:PNMISC>2.0.CO;2.

Frost, B.R., and Frost, C.D., 2008, A geochemical classification for feldspathic igneous rocks: Journal of Petrology, v. 49, p. 1955–1969, https://doi.org/10.1093/petrology/egn054.

Fuston, S., and Wu, J., 2021, Raising the Resurrection plate from an unfolded-slab plate tectonic reconstruction of northwestern North America since early Cenozoic time: Geological Society of America Bulletin, v. 133, p. 1128–1140, https://doi.org/10.1130/B35677.1.

Gale, A., Dalton, C.A., Langmuir, C.H., Su, Y., and Schilling, J.-G., 2013, The mean composition of ocean ridge basalts: Geochemistry, Geophysics, Geosystems, v. 14, p. 489–518, https://doi.org/10.1029/2012GC004334.

Garver, J.I., and Davidson, C.M., 2015, Southwestern Laurentian zircons in Upper Cretaceous flysch of the Chugach–Prince

William terrane in Alaska: American Journal of Science, v. 315, p. 537–556, https://doi.org/10.2475/06.2015.02.

Gasser, D., Bruand, E., Stüwe, K., Foster, D.A., Schuster, R., Fügenschuh, B., and Pavlis, T., 2011, Formation of a metamorphic complex along an obliquely convergent margin: Structural and thermochronological evolution of the Chugach metamorphic complex, southern Alaska: Tectonics, v. 30, TC2012, https://doi.org/10.1029/2010TC002776.

Gasser, D., Rubatto, D., Bruand, E., and Stüwe, K., 2012, Large-scale, short-lived metamorphism, deformation, and magmatism in the Chugach metamorphic complex, southern Alaska: A SHRIMP U-Pb study of zircons: Geological Society of America Bulletin, v. 124, p. 886–905, https://doi.org/10.1130/B30507.1.

Geen, A.C., and Canil, D., 2023, Pattern and source of unusually high-temperature metamorphism in an Eocene forearc recorded by the Pacific Rim terrane, British Columbia, Canada: Journal of Metamorphic Geology, v. 41, p. 583–602, https://doi.org/10.1111/jmg.12709.

Gehrels, G., and Pecha, M., 2014, Detrital zircon U-Pb geochronology and Hf isotope geochemistry of Paleozoic and Triassic passive margin strata of western North America: Geosphere, v. 10, p. 49–65, https://doi.org/10.1130/GES00889.1.

Gehrels, G.E., Valencia, V.A., and Ruiz, J., 2008, Enhanced precision, accuracy, efficiency, and spatial resolution of U-Pb ages by laser ablation–multicollector–inductively coupled plasma–mass spectrometry: Geochemistry, Geophysics, Geosystems, v. 9, Q03017, https://doi.org/10.1029/2007GC001805.

González Guillot, M., Ghiglione, M., Escaloya, M., Pimentel, M.M., Mortensen, J., and Acevedo, R., 2018, Ushuaia pluton: Magma diversification, emplacement and relation with regional tectonics in the southernmost Andes: Journal of South American Earth Sciences, v. 88, p. 497–519, https://doi.org/10.1016/j.jsames.2018.10.001.

Groome, W.G., Thorkelson, D.J., Friedman, R.M., Mortensen, J.K., Massey, N.W.D., Marshall, D.D., and Layer, P.W., 2003, Magmatic and tectonic history of the Leech River complex, Vancouver Island, British Columbia: Evidence for ridge-trench intersection and accretion of the Crescent terrane, *in* Sisson, V.B., Roeske, S.M., and Pavlis, T.L., eds., Geology of a Transpressional Orogen Developed during Ridge-Trench Interaction along the North Pacific Margin: Geological Society of America Special Paper 371, p. 327–354, https://doi.org/10.1130/0-8137-2371-X.327.

Haeussler, P.J., Bradley, D., Goldfarb, R., Snee, L., and Taylor, C., 1995, Link between ridge subduction and gold mineralization in southern Alaska: Geology, v. 23, p. 995–998, https://doi.org/10.1130/0091-7613(1995)023<0995:LBRSAG>2.3.CO;2.

Haeussler, P.J., Bradley, D.C., Wells, R.E., and Miller, M.L., 2003, Life and death of the Resurrection plate: Evidence for its existence and subduction in the northeastern Pacific in Paleocene–Eocene time: Geological Society of America Bulletin, v. 115, p. 867–880, https://doi.org/10.1130/0016-7606(2003)115<0867:LADOTR>2.0.CO;2.

Haeussler, P.J., Gehrels, G.E., and Karl, S.M., 2006, Constraints on the Age and Provenance of the Chugach Accretionary Complex from Detrital Zircons in the Sitka Graywacke near Sitka, Alaska: U.S. Geological Survey Professional Paper 1709-F, 24 p., https://doi.org/10.3133/pp1709F.

Harris, N.R., Sisson, V.B., Wright, J.E., and Pavlis, T.L., 1996, Evidence for Eocene mafic underplating during fore-arc intrusive activity, eastern Chugach Mountains, Alaska: Geology, v. 24, p. 263–266, https://doi.org/10.1130/0091-7613(1996)024<0263:EFEMUD>2.3.CO;2.

Hastie, A.R., 2021, Adakites, *in* Alderton, D., and Elias, S.A., eds., Encyclopedia of Geology (2nd ed.): Oxford, UK, Academic Press, p. 209–214, https://doi.org/10.1016/B978-0-12-409548-9.12496-0.

Hill, M., Morris, J., and Whelan, J., 1981, Hybrid granodiorites intruding the accretionary prism, Kodiak, Shumagin, and Sanak Islands, southwest Alaska: Journal of Geophysical Research: Solid Earth, v. 86, p. 10,569–10,590, https://doi.org/10.1029/JB086iB11p10569.

Hofmann, A.W., 1988, Chemical differentiation of the Earth: The relationship between mantle, continental crust, and oceanic crust: Earth and Planetary Science Letters, v. 90, p. 297–314, https://doi.org/10.1016/0012-821X(88)90132-X.

Hofmann, A.W., 1997, Mantle geochemistry: The message from oceanic volcanism: Nature, v. 385, p. 219–229, https://doi.org/10.1038/385219a0.

Hollister, L.S., 1979, Metamorphism and crustal displacements: New insights: Episodes (Journal of International Geoscience), v. 2, p. 3–8, https://doi.org/10.18814/epiiugs/1979/v2i3/001.

Hudson, T., Plafker, G., and Lanphere, M.A., 1977, Intrusive rocks of the Yakutat–St. Elias area, south-central Alaska: Journal of Research of the U.S. Geological Survey, v. 5, p. 155–172.

Hudson, T., Plafker, G., and Peterman, Z.E., 1979, Paleogene anatexis along the Gulf of Alaska margin: Geology, v. 7, p. 573–577, https://doi.org/10.1130/0091-7613(1979)7<573:PAATGO>2.0.CO;2.

Jacobsen, S.B., and Wasserburg, G.J., 1980, Sm-Nd isotopic evolution of chondrites: Earth and Planetary Science Letters, v. 50, p. 139–155, https://doi.org/10.1016/0012-821X(80)90125-9.

Johnson, S.Y., 1984, Evidence for a margin-truncating transcurrent fault (pre-late Eocene) in western Washington: Geology, v. 12, p. 538–541, https://doi.org/10.1130/0091-7613(1984)12<538:EFAMTF>2.0.CO;2.

Karig, D.E., Caldwell, J.G., and Parmentier, E.M., 1976, Effects of accretion on the geometry of the descending lithosphere: Journal of Geophysical Research: Solid Earth and Planets, v. 81, p. 6281–6291, https://doi.org/10.1029/JB081i035p06281.

Kay, R.W., 1978, Aleutian magnesian andesites: Melts from subducted Pacific Ocean crust: Journal of Volcanology and Geothermal Research, v. 4, p. 117–132, https://doi.org/10.1016/0377-0273(78)90032-X.

Kay, S.M., Jicha, B.R., Citron, G.L., Kay, R.W., Tibbetts, A.K., and Rivera, T.A., 2019, The calc-alkaline Hidden Bay and Kagalaska plutons and the construction of the central Aleutian oceanic arc crust: Journal of Petrology, v. 60, p. 393–439, https://doi.org/10.1093/petrology/egy119.

Kusky, T.M., Bradley, D.C., Donely, D.T., and Rowley, P.J., 2003, Controls on intrusion of near-trench magmas of the Sanak-Baranof belt, Alaska, during Paleogene ridge subduction, and consequences for forearc evolution, *in* Sisson, V.B., Roeske, S.M., and Pavlis, T.L., eds., Geology of a Transpressional Orogen Developed during Ridge-Trench Interaction along the North Pacific Margin: Geological Society of America Special Paper 371, p. 269–292, https://doi.org/10.1130/0-8137-2371-X.269.

Lackey, J.S., Cecil, M.R., Windham, C.J., Frazer, R.E., Bindeman, I.N., and Gehrels, G.E., 2012, The Fine Gold intrusive suite: The roles of basement terranes and magma source development in the Early Cretaceous Sierra Nevada Batholith: Geosphere, v. 8, p. 292–313, https://doi.org/10.1130/GES00745.1.

Lagabrielle, Y., Guivel, C., Maury, R.C., Bourgois, J., Fourcade, S., and Martin, H., 2000, Magmatic-tectonic effects of high thermal regime at the site of active ridge subduction: The Chile triple junction model: Tectonophysics, v. 326, p. 255–268, https://doi.org/10.1016/S0040-1951(00)00124-4.

Lempert, R., Crowley, P.D., Davidson, C., and Garver, J.I., 2015, Geochemical and petrologic evidence for magma mixing in the Sheep Bay and McKinley Peak plutons, Prince William Sound, Alaska: Geological Society of America Abstracts with Programs, v. 47, no. 4, p. 59.

Little, T.A., and Naeser, C.W., 1989, Tertiary tectonics of the Border Ranges fault system, Chugach Mountains, Alaska: Deformation and uplift in a forearc setting: Journal of Geophysical Research: Solid Earth, v. 94, p. 4333–4359, https://doi.org/10.1029/JB094iB04p04333.

Loney, R.A., Brew, D.A., Muffler, L.J.P., and Pomeroy, J.S., 1975, Reconnaissance Geology of Chichagof, Baranof, and Kruzof Islands, Southeastern Alaska: U.S. Geological Survey Professional Paper 792, 105 p., https://doi.org/10.3133/pp792.

Luffi, P., and Ducea, M.N., 2022, Chemical mohometry: Assessing crustal thickness of ancient orogens using geochemical and isotopic data: Reviews of Geophysics, v. 60, https://doi.org/10.1029/2021RG000753.

Lull, J.S., and Plafker, G., 1990, Geochemistry and paleotectonic implications of metabasaltic rocks in the Valdez Group, southern Alaska, *in* Dover, J.H., and Galloway, J.P., eds., Geologic Studies in Alaska by the U.S. Geological Survey, 1989: U.S. Geological Survey Bulletin 1946, p. 29–38, https://doi.org/10.3133/b1946.

Lytwyn, J., Casey, J., Gilbert, S., and Kusky, T., 1997, Arc-like mid-ocean ridge basalt formed seaward of a trench-forearc system just prior to ridge subduction: An example from subaccreted ophiolites in southern Alaska: Journal of Geophysical Research: Solid Earth, v. 102, p. 10,225–10,243, https://doi.org/10.1029/96JB03858.

Lytwyn, J., Lockhart, S., Casey, J., and Kusky, T., 2000, Geochemistry of near-trench intrusives associated with ridge subduction, Seldovia Quadrangle, southern Alaska: Journal of Geophysical Research: Solid Earth, v. 105, p. 27,957–27,978, https://doi.org/10.1029/2000JB900294.

MacKevett, E.M., and Plafker, G., 1974, The Border Ranges fault in south-central Alaska: Journal of Research of the U.S. Geological Survey, v. 2, p. 323–329.

Madsen, J.K., Thorkelson, D.J., Friedman, R.M., and Marshall, D.D., 2006, Cenozoic to Recent plate configurations in the Pacific Basin: Ridge subduction and slab window magmatism in western North America: Geosphere, v. 2, p. 11–34, https://doi.org/10.1130/GES00020.1.

Maeda, J., and Kagami, H., 1996, Interaction of a spreading ridge and an accretionary prism: Implications from MORB magmatism in the Hidaka magmatic zone, Hokkaido, Japan: Geology, v. 24, p. 31–34, https://doi.org/10.1130/0091-7613(1996)024<0031:IOASRA>2.3.CO;2.

Marshak, R.S., and Karig, D.E., 1977, Triple junctions as a cause for anomalously near-trench igneous activity between the trench and volcanic arc: Geology, v. 5, p. 233–236, https://doi.org/10.1130/0091-7613(1977)5<233:TJAACF>2.0.CO;2.

Martin, H., 1999, Adakitic magmas: Modern analogues of Archaean granitoids: Lithos, v. 46, p. 411–429, https://doi.org/10.1016/S0024-4937(98)00076-0.

Martin, H., Smithies, R.H., Rapp, R., Moyen, J.-F., and Champion, D., 2005, An overview of adakite, tonalite-trondhjemite-granodiorite (TTG), and sanukitoid: Relationships and some implications for crustal evolution: Lithos, v. 79, p. 1–24, https://doi.org/10.1016/j.lithos.2004.04.048.

Middlemost, E.A.K., 1994, Naming materials in the magma/igneous rock system: Earth-Science Reviews, v. 37, p. 215–224, https://doi.org/10.1016/0012-8252(94)90029-9.

Miyashiro, A., 1974, Volcanic rock series in island arcs and active continental margins: American Journal of Science, v. 274, p. 321–355, https://doi.org/10.2475/ajs.274.4.321.

Moore, J.C., Byrne, T., Plumley, P.W., Reid, M., Gibbons, H., and Coe, R.S., 1983, Paleogene evolution of the Kodiak Islands, Alaska: Consequences of ridge-trench interaction in a more southerly latitude: Tectonics, v. 2, p. 265–293, https://doi.org/10.1029/TC002i003p00265.

Müller, R.D., et al., 2019, A global plate model including lithospheric deformation along major rifts and orogens since the Triassic: Tectonics, v. 38, p. 1884–1907, https://doi.org/10.1029/2018TC005462.

Olson, H., Sophis, J., Davidson, C., and Garver, J., 2017, Detrital zircon from the Yakutat terrane: Differentiating the Yakutat Group and the schist of Nunatak Fjord: Geological Society of America Abstracts with Programs, v. 49, https://doi.org/10.1130/abs/2017CD-292889.

Padilla, A.J., and Gualda, G.A.R., 2016, Crystal-melt elemental partitioning in silicic magmatic systems: An example from the Peach Spring Tuff high-silica rhyolite, southwest USA: Chemical Geology, v. 440, p. 326–344, https://doi.org/10.1016/j.chemgeo.2016.07.004.

Pavlis, T.L., and Roeske, S.M., 2007, The Border Ranges fault system, southern Alaska, *in* Ridgway, K.D., Trop, J.M., Glen, J.M.G., and O'Neill, J.M., eds., Tectonic Growth of a Collisional Continental Margin: Crustal Evolution of Southern Alaska: Geological Society of America Special Paper 431, p. 95–127, https://doi.org/10.1130/2007.2431(05).

Pavlis, T.L., and Sisson, V.B., 1995, Structural history of the Chugach metamorphic complex in the Tana River region, eastern Alaska: A record of Eocene ridge subduction: Geological Society of America Bulletin, v. 107, p. 1333–1355, https://doi.org/10.1130/0016-7606(1995)107<1333:SHOTCM>2.3.CO;2.

Pavlis, T.L., and Sisson, V.B., 2003, Development of a subhorizontal decoupling horizon in a transpressional system, Chugach metamorphic complex, Alaska: Evidence for rheological stratification of the crust, *in* Sisson, V.B., Roeske, S.M., and Pavlis, T.L., eds., Geology of a Transpressional Orogen Developed during Ridge-Trench Interaction along the North Pacific Margin: Geological Society of America Special Paper 371, p. 191–216, https://doi.org/10.1130/0-8137-2371-X.191.

Pavlis, T.L., Monteverde, D.H., Bowman, J.R., Rubenstone, J.L., and Reason, M.D., 1988, Early Cretaceous near-trench plutonism in southern Alaska: A tonalite-trondhjemite intrusive complex injected during ductile thrusting along the Border Ranges fault system: Tectonics, v. 7, p. 1179–1199, https://doi.org/10.1029/TC007i006p01179.

Pavlis, T.L., Marty, K., and Sisson, V.B., 2003, Constrictional flow within the Eocene forearc of southern Alaska: An effect of dextral shear during ridge subduction, *in* Sisson, V.B., Roeske, S.M., and Pavlis, T.L., eds., Geology of a Transpressional Orogen Developed during Ridge-Trench Interaction along the North Pacific Margin: Geological Society of America Special Paper 371, p. 171–190, https://doi.org/10.1130/0-8137-2371-X.171.

Plafker, G., 1990, Regional vertical tectonic displacement of shorelines in south-central Alaska during and between great earthquakes: Northwest Science, v. 64, p. 250–258.

Plafker, G., Nokleberg, W.J., and Lull, J.S., 1989, Bedrock geology and tectonic evolution of the Wrangellia, Peninsular, and Chugach terranes along the Trans-Alaska Crustal Transect in the Chugach Mountains and southern Copper River Basin, Alaska: Journal of Geophysical Research: Solid Earth, v. 94, p. 4255–4295, https://doi.org/10.1029/JB094iB04p04255.

Plafker, G., Moore, J.C., and Winkler, G.R., 1994, Geology of the southern Alaska margin, *in* Plafker, G., and Berg, H.C., eds., The Geology of Alaska: Boulder, Colorado, Geological Society of America, The Geology of North America, v. G-1, p. 389–449, https://doi.org/10.1130/DNAG-GNA-G1.389.

Plumley, P.W., Coe, R.S., and Byrne, T., 1983, Paleomagnetism of the Paleocene Ghost Rocks Formation, Prince William terrane, Alaska: Tectonics, v. 2, p. 295–314, https://doi.org/10.1029/TC002i003p00295.

Putnam, R., Glazner, A.F., Coleman, D.S., Kylander-Clark, A.R.C., Pavelsky, T., and Abbot, M.I., 2015, Plutonism in three dimensions: Field and geochemical relations on the southeast face of El Capitan, Yosemite National Park, California: Geosphere, v. 11, p. 1133–1157, https://doi.org/10.1130/GES01133.1.

R Core Team, 2022, Language and Environment for Statistical Computing: Vienna, Austria, The R Foundation for Statistical Computing, https://www.R-project.org/ (last accessed August 2023).

Richter, D.H., Preller, C., Labay, K., and Shew, N., 2006, Geologic Map of the Wrangell–Saint Elias National Park and Preserve, Alaska: U.S. Geological Survey Scientific Investigations Map 2877, scale 1:50,000, https://doi.org/10.3133/sim2877.

Rick, B., 2014, U/Pb dating of detrital zircons, Baranof Island, SE Alaska, *in* Varga, R., ed., 27th Keck Symposium Proceedings Volume: South Hadley, Massachusetts, Keck Geology Consortium, p. 1–7.

Rodríguez, N., Diaz-Alvarado, J., Fernandez, C., Fuentes, P., Breitkreuz, C., and Tassirini, C.C.G., 2019, The significance of U-Pb zircon ages in zoned plutons: The case of the Flamenco pluton, Coastal Range batholith, northern Chile: Geoscience Frontiers, v. 10, p. 1073–1099, https://doi.org/10.1016/j.gsf.2018.06.003.

Salters, V.J.M., and Stracke, A., 2004, Composition of the depleted mantle: Geochemistry, Geophysics, Geosystems, v. 5, Q05B07, https://doi.org/10.1029/2003GC000597.

Sample, J.C., and Reid, M.R., 2003, Large-scale, latest Cretaceous uplift along the northeast Pacific Rim: Evidence from sediment volume, sandstone petrography, and Nd isotope signatures of the Kodiak Formation, Kodiak Islands, Alaska, *in* Sisson, V.B., Roeske, S.M., and Pavlis, T.L., eds., Geology of a Transpressional Orogen Developed during Ridge-Trench Interaction along the North Pacific Margin: Geological Society of America Special Paper 371, p. 51–70, https://doi.org/10.1130/0-8137-2371-X.51.

Samson, S.D., Patchett, P.J., McClelland, W.C., and Gehrels, G.E., 1991, Nd and Sr isotopic constraints on the petrogenesis of the west side of the northern Coast Mountains batholith, Alaskan and Canadian Cordillera: Canadian Journal of Earth Sciences, v. 28, p. 939–946, https://doi.org/10.1139/e91-085.

Schartman, A., Enkelmann, E., Garver, J.I., and Davidson, C.M., 2019, Uplift and exhumation of the Russell Fiord and Boundary blocks along the northern Fairweather transform fault, Alaska: Lithosphere, v. 11, p. 232–251, https://doi.org/10.1130/L1011.1.

Seyler, C.E., Kirkpatrick, J.D., Faber, C., Licht, A., Šilerová, D., and Regalla, C., 2022, Structural and metamorphic history of the Leech River shear zone, Vancouver Island, British Columbia: Tectonics, v. 41, https://doi.org/10.1029/2021TC007132.

Shand, S.J., 1951, Eruptive Rocks: New York, John Wiley, 488 p.

Shephard, G.E., Müller, R.D., and Seton, M., 2013, The tectonic evolution of the Arctic since Pangea breakup: Integrating constraints from surface geology and geophysics with mantle structure: Earth-Science Reviews, v. 124, p. 148–183, https://doi.org/10.1016/j.earscirev.2013.05.012.

Shinjoe, H., Orihashi, Y., Niki, S., Sato, A., Sasaki, M., Sumii, T., and Hirata, T., 2021, Zircon U-Pb ages of Miocene granitic rocks in the Koshikijima Islands: Implications for Neogene tectonics in the Kyushu region, southwest Japan: The Island Arc, v. 30, https://doi.org/10.1111/iar.12383.

Sisson, T.W., and Bacon, C.R., 1992, Garnet/high-silica rhyolite trace element partition coefficients measured by ion microprobe: Geochimica et Cosmochimica Acta, v. 56, p. 2133–2136, https://doi.org/10.1016/0016-7037(92)90336-H.

Sisson, V.B., and Pavlis, T.L., 1993, Geologic consequences of plate reorganization: An example from the Eocene southern Alaska fore arc: Geology, v. 21, p. 913–916, https://doi.org/10.1130/0091-7613(1993)021<0913:GCOPRA>2.3.CO;2.

Sisson, V.B., Hollister, L.S., and Onstott, T.C., 1989, Petrologic and age constraints on the origin of a low-pressure/high-temperature metamorphic complex, southern Alaska: Journal of Geophysical Research: Solid Earth, v. 94, p. 4392–4410, https://doi.org/10.1029/JB094iB04p04392.

Sisson, V.B., Pavlis, T.L., Roeske, S.M., and Thorkelson, D.J., 2003a, Introduction: An overview of ridge-trench interactions in modern and ancient settings, *in* Sisson, V.B., Roeske, S.M., and Pavlis, T.L., eds., Geology of a Transpressional Orogen Developed during Ridge-Trench Interaction along the North Pacific Margin: Geological Society of America Special Paper 371, p. 1–18, https://doi.org/10.1130/0-8137-2371-X.1.

Sisson, V.B., Poole, A.R., Harris, N.R., Burner, H.C., Pavlis, T.L., Copeland, P., Donelick, R.A., and McLelland, W.C., 2003b, Geochemical and geochronologic constraints for genesis of a tonalite-trondhjemite suite and associated mafic intrusive rocks in the eastern Chugach Mountains, Alaska: A record of ridge-transform subduction, *in* Sisson, V.B., Roeske, S.M., and Pavlis, T.L., eds., Geology of a Transpressional Orogen Developed during Ridge-Trench Interaction along the North Pacific Margin: Geological Society of America Special Paper 371, p. 293–326, https://doi.org/10.1130/0-8137-2371-X.293.

Smart, K.J., Pavlis, T.L., Sisson, V.B., Roeske, S.M., and Snee, L.W., 1996, The Border Ranges fault system in Glacier Bay National Park, Alaska: Evidence for major early Cenozoic dextral strike-slip motion: Canadian Journal of Earth Sciences, v. 33, p. 1268–1282, https://doi.org/10.1139/e96-096.

Sun, S.-S., and McDonough, W.F., 1989, Chemical and isotopic systematics of oceanic basalts: Implications for mantle composition and processes, *in* Saunders, A.D., and Norry, M.J.,

eds., Magmatism in the Ocean Basins: Geological Society, London, Special Publication 42, p. 313–345, https://doi.org/10.1144/GSL.SP.1989.042.01.19.

Thorkelson, D.J., 1996, Subduction of diverging plates and the principles of slab window formation: Tectonophysics, v. 255, p. 47–63, https://doi.org/10.1016/0040-1951(95)00106-9.

Thorkelson, D.J., and Breitsprecher, K., 2005, Partial melting of slab window margins: Genesis of adakitic and non-adakitic magmas: Lithos, v. 79, p. 25–41, https://doi.org/10.1016/j.lithos.2004.04.049.

Vernon, R.H., 1984, Microgranitoid enclaves in granites—Globules of hybrid magma quenched in a plutonic environment: Nature, v. 309, p. 438–439, https://doi.org/10.1038/309438a0.

Wackett, A.A., 2014, Petrology and Geochemistry of the Crawfish Inlet and Krestof Island Plutons, Baranof Island, Alaska [Geosciences Student Honor's Thesis]: San Antonio, Texas, Trinity University, 101 p.

Webster, J.D., and Piccoli, P.M., 2015, Magmatic apatite: A powerful, yet deceptive, mineral: Elements, v. 11, p. 177–182, https://doi.org/10.2113/gselements.11.3.177.

Wells, R., Bukry, D., Friedman, R., Pyle, D., Duncan, R., Haeussler, P., and Wooden, J., 2014, Geologic history of Siletzia, a large igneous province in the Oregon and Washington Coast Range: Correlation to the geomagnetic polarity time scale and implications for a long-lived Yellowstone hotspot: Geosphere, v. 10, p. 692–719, https://doi.org/10.1130/GES01018.1.

White, A.J.R., Clemens, J.D., Holloway, J.R., Silver, L.T., Chappell, B.W., and Wall, V.J., 1986, S-type granites and their probable absence in southwestern North America: Geology, v. 14, p. 115–118, https://doi.org/10.1130/0091-7613(1986)14<115:SGATPA>2.0.CO;2.

Wilson, F.H., Hults, C.P., Mull, C.G., and Karl, S.M., 2015, Geologic Map of Alaska: U.S. Geological Survey Scientific Investigations Map 3340, scale 1:250,000, https://doi.org/10.3133/sim3340.

Wyllie, P.J., Cox, K.G., and Biggar, G.M., 1962, The habit of apatite in synthetic systems and igneous rocks: Journal of Petrology, v. 3, p. 238–243, https://doi.org/10.1093/petrology/3.2.238.

Xu, J.-F., Shinjo, R., Defant, M.J., Wang, Q., and Rapp, R.P., 2002, Origin of Mesozoic adakitic intrusive rocks in the Ningzhen area of east China: Partial melting of delaminated lower continental crust?: Geology, v. 30, p. 1111–1114, https://doi.org/10.1130/0091-7613(2002)030<1111:OOMAIR>2.0.CO;2.

Yogodzinski, G.M., Lees, J.M., Churikova, T.G., Dorendorf, F., Wöerner, G., and Volynets, O.N., 2001, Geochemical evidence for the melting of subducting oceanic lithosphere at plate edges: Nature, v. 409, p. 500–504, https://doi.org/10.1038/35054039.

Zindler, A., and Hart, S., 1986, Chemical geodynamics: Annual Review of Earth and Planetary Sciences, v. 14, p. 493–571, https://doi.org/10.1146/annurev.ea.14.050186.002425.

Zuffa, G.G., Nilsen, T.H., and Winkler, G.R., 1980, Rock-Fragment Petrography of the Upper Cretaceous Chugach Terrane, Southern Alaska: U.S. Geological Survey Open-File Report 80–713, 28 p., https://doi.org/10.3133/ofr80713.

Zumsteg, C.L., Himmelberg, G.R., Karl, S.M., and Haeussler, P.J., 2003, Metamorphism within the Chugach accretionary complex on southern Baranof Island, southeastern Alaska: Geology of a transpressional orogen developed during ridge-trench interaction along the North Pacific margin, *in* Sisson, V.B., Roeske, S.M., and Pavlis, T.L., eds., Geology of a Transpressional Orogen Developed during Ridge-Trench Interaction along the North Pacific Margin: Geological Society of America Special Paper 371, p. 253–268, https://doi.org/10.1130/0-8137-2371-X.253.